Journal of Power Sources 639 (2025) 236661

Contents lists available at ScienceDirect

Journal of Power Sources

journal homepage: www.elsevier.com/locate/jpowsour

From waste to fuel cells. *In situ* preparation of an atomically precise Pd (II)-catalyst by selective extraction of Pd(II) from a mixture of metal ions using modified multi walled carbon nanotubes (MWCNTs) and its implementation in the oxygen reduction reaction (ORR) in alkaline solution

Marco Bonechi [a,b,1], Carlotta Cappanni [a,1], Pietro Gentilesca [a,1], Carla Bazzicalupi [a,*], Walter Giurlani [a,b], Massimo Innocenti [a,b,**], Leonardo Lari [c,d], Francesco Montanari [a], Matteo Savastano [b,e,***], Mirko Severi [a], Antonio Bianchi [a,b]

[a] Department of Chemistry "Ugo Schiff", University of Florence, Via Della Lastruccia 3-13, 50019, Sesto Fiorentino, Italy
[b] National Interuniversity Consortium of Materials Science and Technology (INSTM), Research Unit of Florence, Via G. Giusti 9, 50121, Florence, Italy
[c] School of Physics, Engineering and Technology, University of York, Heslington, York, YO10 5DD, UK
[d] The York-JEOL Nanocentre, University of York, Heslington, York, YO10 5BR, UK
[e] Department for the Promotion of Human Science and Quality of Life, University San Raffaele Roma, Via di Val Cannuta 247, 00166, Rome, Italy

HIGHLIGHTS

- An efficient Pd catalyst for ORR was prepared following a circular economy criterion.
- The catalyst was prepared via selective extraction of Pd(II) from wastewater.
- The catalysts is assembled via Pd uptake on modified multi-walled carbon nanotubes.
- The heterogeneous catalyst is very efficient despite the low Pd(II) loading (1.94 %).
- Four-electron reduction of O_2 was achieved with almost exclusive production of H_2O.

GRAPHICAL ABSTRACT

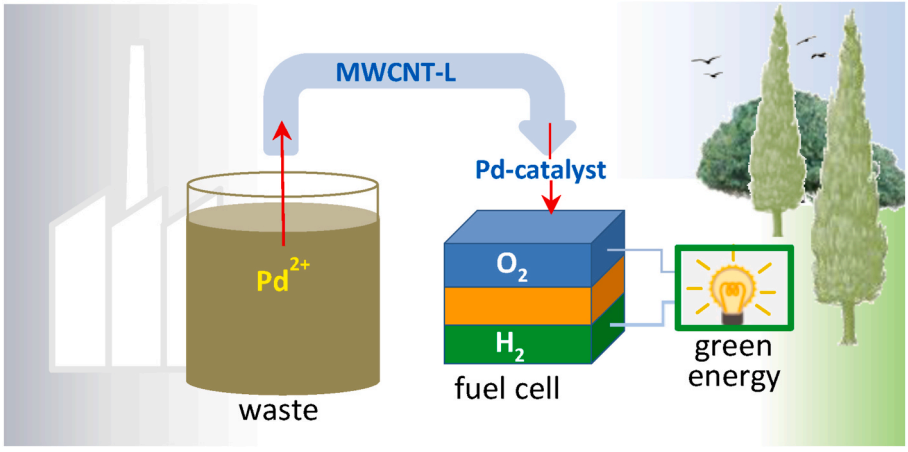

* Corresponding author.
** Corresponding author. Department of Chemistry "Ugo Schiff", University of Florence, Via Della Lastruccia 3-13, 50019, Sesto Fiorentino, Italy.
*** Corresponding author. Department for the Promotion of Human Science and Quality of Life, University San Raffaele Roma, Via di Val Cannuta 247, 00166, Rome, Italy.
E-mail addresses: carla.bazzicalupi@unifi.it (C. Bazzicalupi), m.innocenti@unifi.it (M. Innocenti), matteo.savastano@uniroma5.it (M. Savastano).
[1] These authors contributed equally.

https://doi.org/10.1016/j.jpowsour.2025.236661
Received 27 November 2024; Received in revised form 31 January 2025; Accepted 26 February 2025
Available online 6 March 2025

ARTICLE INFO

Keywords:
Carbon nanotubes
ORR
Palladium recovery
Wastewater treatment
RRDE

ABSTRACT

Fuel cells can effectively mitigate environmental challenges by enabling clean energy production. A significant obstacle to the implementation of fuel cells is the need for catalysts that make the electrode reactions efficient, especially the oxygen reduction reaction (ORR), allowing to replace the currently used bulk platinum electrodes which are efficient but very expensive. In this paper, we demonstrate that an atomically precise and very efficient Pd(II)-based catalyst for ORR can be easily prepared under environmentally friendly conditions using non-covalently modified multi-walled carbon nanotubes (MWCNT-L) to selectively recover precious Pd(II) from wastewater. Electrodes loaded with the new MWCNT-LPd catalyst, which contains only 1.94 % of Pd(II), give rise to ORR with 90 % H_2O production (4 e^- process), onset potential of 0.846 V (vs RHE) and half-wave potential ($E_{1/2}$) of 0.657 V, very close to the performance of bulk platinum electrodes. Sustainable energy production and waste management are combined here within the framework of a circular economy criterion that places emphasis on environment protection.

1. Introduction

Clean energy production and waste management are an inescapable binomial for the sustainability of all human activities, future competitiveness and development. As regards waste management, a convenient approach consists in recovering/regenerating waste for reuse as part of a circular economy that valorises those materials that have reached the end of their life cycle and would otherwise be destined for landfill. The first term of this binomial, the production of clean energy, has a double link with waste management since its primary objective is to avoid waste production and because it could be nourished with waste according to the circular economy criterion mentioned above [1,2]. The main goal of clean energy is to move away from fossil fuels and current trends to achieve this goal are the use of energy sources that regenerate naturally over time and do not run out, the so-called renewable energies [3–6], and the development of technologies based on clean fuels such as fuel cells and hydrogen [6–12].

In this paper we address these issues simultaneously. We report the preparation of a new atomically precise heterogeneous catalyst containing Pd(II) ions anchored on multi walled carbon nanotubes (MWCNTs) and the results of its application in accelerating the oxygen reduction reaction (ORR), which is the fundamental, albeit sluggish, process occurring at the cathode in proton exchange membrane fuel cells. We also show that this efficient catalyst can be obtained by selective and quantitative extraction of Pd(II) from a mixture of metal ions that typically accompany Pd(II) in wastewaters resulting from the processing of this metal, which is precious but also very toxic when it is in the form of Pd(II) [12–15]. It is therefore very important, both from an economic and a health point of view, to purify wastewater from Pd(II) and recover this metal. Several methods have been developed or proposed for the recovery of Pd(II), which are often expensive and energy- and labour-intensive, especially if implemented in environmentally friendly ways [6–22]. Various processes, especially hydrometallurgical ones [23–25], convert solid waste into Pd(II)-containing solutions and recover the dissolved metal by different methods such as membrane separation [26], precipitation [27], liquid–liquid extraction [28–30], ion exchange [31], selective coordination with functionalized materials [32] or adsorption [33,34].

The method we are suggesting here is intended for the *in situ* conversion of a Pd(II) waste (an acidic solution containing Pd(II) and other typical metal ions) to an ORR catalyst of high added value. This was made possible by the appropriate choice of the ligand used to functionalize the surface of the MWCNTs and the whole process to assemble the catalyst (MWCNT-LPd) is conducted in very environmentally friendly conditions, occurs spontaneously in water, at room temperature, does not need a protected atmosphere and requires only minimal energy consumption.

Platinum metal electrodes continue to be the prime choice for accelerating the slow ORR, due to their high catalytic performance [35–38], but the poor availability and the high price of this metal make these electrodes not economically viable to satisfy the large energy demand of today's society. Other strategies that employ less expensive non-noble transition metals [38–44], non-metallic electrodes [44–48] or atomically precise electrocatalysts [49–57] are being thoroughly investigated as alternatives to platinum metal electrodes. Among these, atomically precise electrocatalysts are attracting particular interest due to their high atomic utilization efficiency, special electronic structure and homogeneous distribution of active centres [49–57]. Although atomically precise electrocatalysts can often be based on precious metals, the loadings of these expensive components are so low that they still represent a low-cost alternative.

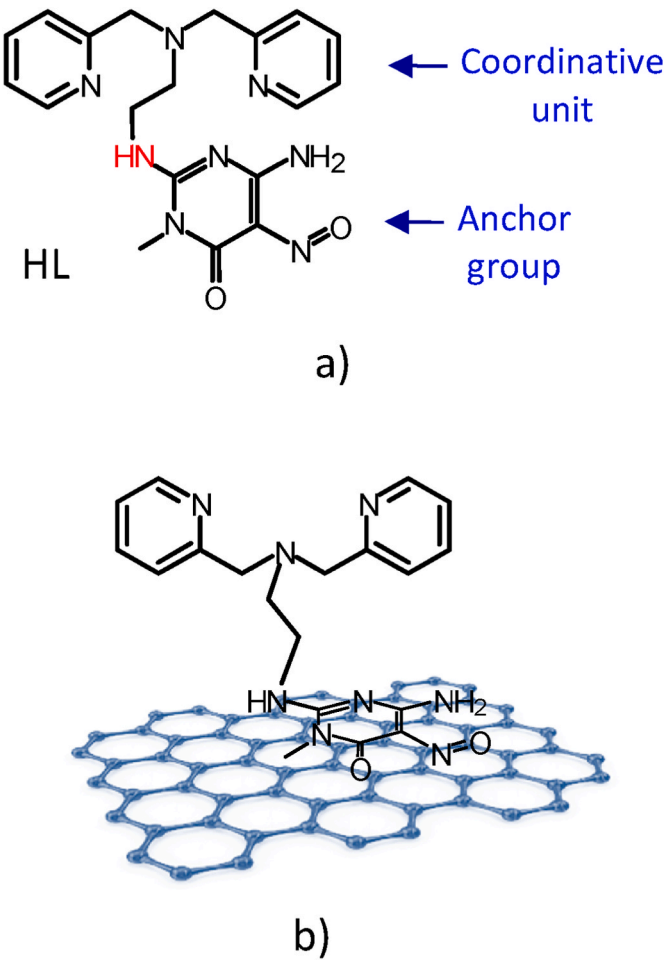

Fig. 1. a) The HL ligand composed of a binding unit for the coordination of metal ions and an anchor group for attachment onto graphene surfaces. b) Schematic representation of the anchorage of HL on a graphene surface.

The ligand used in the present work to functionalize the surface of MWCNTs and capture Pd(II) ions is shown in Fig. 1a. The 6-amino-3,4-dihydro-3-methyl-5-nitroso-4-oxopyrimidine residue is the anchor group responsible for the non-covalent adhesion on MWCNTs (Fig. 1b). This group, which in water gives rise to spontaneous and irreversible adhesion on graphene surfaces via π-π stacking, was originally employed for the preparation of functionalized activated carbon for the extraction of chromate anions from aqueous solutions [58] and successively extended to the production of similar hybrid materials for the removal of further anions and metal cations from water [59–61,62–64], as well as for the construction of metal-based catalysts for applications in Sonogashira cross-coupling reactions [65–67], hydrogenation processes [68], photochemical generation of hydrogen [69], and ORR for fuel cells [70–74].

The remaining tridentate portion of the molecule is responsible for metal chelation: it forms a Pd(II) complex sufficiently stable to resist demetallation processes, for optimal operation of the catalyst in the ORR in alkaline media, but does not add kinetic impediments to the complexation of this metal ion, which itself is slow to form complexes, that could be detrimental for its selective extraction from a mixture of metal ions. A more stable complex could have been obtained by using of a macrocyclic ligand, rather than an open-chain one, yet the rate of Pd (II) complexation could have been slowed down too much compared to other metal ions. Another reason for the choice of this ligand was the presence of two pyridine groups which favour the complexation of soft Pd(II) ions compared to harder metal ions.

2. Experimental

2.1. Materials

All starting materials were high purity compounds purchased from commercial sources and were used without further purification. The HL ligand was synthetized as previously described [75]. Graphitized MWCNTs (99.9 % C, outer diameter 8–15 nm, inner diameter 3–5 nm, specific surface area 117 m^2/g) were purchased from NanoAmor (Texas, USA).

2.2. Potentiometric measurements

Ligand protonation constants and stability constants of the Cu(II) complexes were determined by means of potentiometric (pH-metric) titrations in 0.1 M NMe_4Cl aqueous solution at 298.1 ± 0.1 K using an automated apparatus and a procedure previously described [76]. Emf data acquisition was performed with the computer program PASAT [77,78]. The combined electrode (Metrohm 6.0262.100) was calibrated as a hydrogen-ion concentration probe by titration of known amounts of HCl with CO_2-free NaOH solutions and determining the equivalent point by Gran's method [79], which furnished the standard potential, E°, and the ionic product of water (pK_w = 13.83(1) in 0.1 M NMe_4Cl at 298.1 K). The concentration of HL ligand was about $1•10^{-3}$ M in all experiments and the studied pH range was 2.0–11.5. A preliminary study of the Cu (II)/HL system showed that Cu(II) complexes are already formed in very acidic solutions, *i.e.* protonation of the ligand does not provide enough competition with metal complexation and the use of an additional competitor (a second ligand) was necessary to carry out the determination of the stability constants. The competitor we chose was the tripodal ligand tris(2-aminoethyl)amine which was used in about $1•10^{-3}$ M concentration. The concentration of Cu(II) was in the range $5•10^{-4}$-$1•10^{-3}$ M. Three measurements were performed and used to determine the protonation constants and three measurements to determine complexation constants. Equilibrium constants were calculated from the potentiometric data using the HYPERQUAD [80] computer program. The equilibrium constants for Cu(II) complexation with tris (2-aminoethyl)amine, used in the analysis of competitive complexation experiments, were redetermined under the present experimental conditions using the protonation constants of tris(2-aminoethyl)amine we had previously determined [81]: the values obtained ($\log K_{CuL}$ = 18.92, $\log K_{CuLH-1}$ = 9.76) are in good agreement with literature values available for similar (not identical) experimental conditions [82].

2.3. Crystal structure determination of $[Cu(HL)Cl_2]$, $[Zn(HL)Cl_2]$ and $[Pd(HL)Cl]Cl·5H_2O$

Blue crystals of $[Cu(HL)Cl_2]$ and violet crystals of $[Zn(HL)Cl_2]$ suitable for X-ray diffraction analysis (XRD) were obtained by slow evaporation at room temperature of water:ethanol 50:50 (v:v) solutions containing HL and MCl_2 (M = Cu, Zn) in equimolar amounts. Metal ions were dosed using standardized stock solutions. Orange crystals of $[Pd(HL)Cl]Cl·5H_2O$ suitable for X-ray analysis were obtained from an aqueous solution, at pH 3, containing equimolar quantities of HL and K_2PdCl_4 after boiling for a few minutes, cooling to room temperature and slow evaporation. Satisfactory elemental analyses were obtained for the three compounds. The integrated intensities were corrected for Lorentz and polarization effects and an empirical absorption correction (SADABS) [83] was applied. $[Cu(HL)Cl_2]$ and $[Zn(HL)Cl_2]$ crystallize in the chiral space group $P2_12_12_1$, despite they are not chiral compounds, and their structures were refined as inversion twins. The three crystal structures were solved by direct methods (SHELXS) [84] and refinements were performed by means of full-matrix least-squares using SHELXL Version 2019/3 [85]. Non-H atoms were anisotropically refined. H atoms were introduced as riding atoms with thermal parameter calculated in agreement with the linked atom. The amine hydrogen of the arm bearing the pyrimidine pendant (red in Fig. 1a), the aromatic amine hydrogen atoms and the water hydrogen atoms (palladium structure) were located in the Fourier difference maps, included in the calculations and freely refined. A summary of the crystallographic and refinement data is reported in Table S1. Molecular plots were obtained using the software CCDC Mercury [86]. Crystallographic data have been deposited at the Cambridge Crystallographic Data Centre (CCDC 2392535, 2392536, 2392537).

2.4. Spectrophotometric measurements

UV–Vis absorption spectra were recorded at 298 K by using a Jasco V-670 spectrophotometer. Spectra of HL were recorded in the pH range 0.8–12.6 with HL concentration of $2.0•10^{-5}$ M. UV–Vis spectra of the Cu (II) complex were recorded in the pH range 0.9–12.1 with HL and Cu(II) concentrations of $2.0•10^{-5}$ M.

UV–Vis spectra of the Pd(II) complex were recorded in the pH range 1.1–12.0 with HL and Pd(II) (as K_2PdCl_4) concentrations of $2.0•10^{-5}$ M. A stock solution containing ligand and metal ion (concentrations given above) was prepared at pH 3, to avoid formation of metal hydroxides/oxides, and allowed to equilibrate. The UV–Vis spectrum of this solution was checked daily until the invariance was reached. This stock solution was used to prepare solutions at different pH in the above range (pH 1.1–12.0) which were allowed to equilibrate for 8 days. The recorded pH of these solutions was measured after the equilibrium was reached.

2.5. Preparation of the MWCNT-L material

The conditions for the preparation of the MWCNT-L hybrid material were chosen after determining the adsorption isotherm of HL on MWCNT under unprotected atmosphere, at 298.1 K, in water, at pH 9 where HL is in its neutral (not ionic) form. The obtained isotherm (Fig. S1) shows that after fast formation of a monolayer the system presents a significant tendency towards multilayer adsorption (type II isotherm). The conditions adopted for the preparation of MWCNT-L (replicating the isotherm point indicated by a red arrow in Fig. S1) were chosen in order to obtain the maximum coverage of the MWCNT surface while limiting the formation of multilayers. Accordingly, the MWCNT-L hybrid material was prepared in water (pH 9), at room

temperature, in unprotected atmosphere: 200 mg of MWCNTs were suspended in 200 cm^3 of a $4\bullet10^{-4}$ M solution of HL at pH 9 and the resulting suspension was kept under stirring during 72 h. The solid (MWCNT-L) was then collected by filtration, washed with water and dried under reduced pressure, at room temperature and in the presence of a desiccant (NaOH) until constant weight. The amount of HL remained in solution was measured by means of UV spectroscopy (Fig. S2) and used to determine the loading of ligand (0.205 mmol/g) in the MWCNT-L hybrid material. 180 mg of this compound was then suspended in 180 cm^3 of water (pH 5), kept under stirring during 72 h at room temperature, filtered and dried under reduced pressure, at room temperature and in the presence of a desiccant (NaOH) until constant weight. The amount of HL remained in MWCNT-L after the desorption experiment (0.182 mmol/g) was determined by measuring the concentration of ligand desorbed into the solution by means of UV spectroscopy (Fig. S2).

2.6. Metal extraction

Metal ion extraction experiments with the above MWCNT-L material (ligand content: 0.182 mmol/g) were performed using a mother solution, at pH 4, composed of Pd(II), Cu(II), Co(II), Ni(II), Zn(II) and Cd(II), each in 1.0 mM concentration, prepared from stock solutions of chloride salts of each metal ion except for Pd(II) which was added as solid K_2PdCl_4. The final chloride concentration was 14.0 mM. Aliquots of this solution were taken into separate vials and added with the quantity of MWCNT-L necessary to provide 1 equivalent of ligand per 1 metal ion. The suspensions were sonicated for few seconds and then kept under stirring at 298 K. The suspensions were taken after measured intervals of time (from 2 h to 240 h), immediately filtered and the solutions' content was analysed by ICP-OES (Inductively Coupled Plasma – Optical Emission spectrometry). Blank experiments were performed to exclude possible adsorption of metal ions by the plastic vials and to confirm the composition of the mother solution.

For ICP-OES analysis, the above samples were diluted 50-fold to a total volume of 5.0 mL using ultrapure water (MilliQ – resistivity >18 MΩ cm). The determination of Cu, Co, Ni, Zn, Cd and Pd concentrations in the samples was performed in triplicate using a Varian 720-ES Inductively Coupled Plasma Atomic Emission Spectrometer. 5.0 mL of each sample were spiked with 1.0 ppm of Ge used as an internal standard, and analysed. Calibration standards were prepared by gravimetric serial dilution from commercial stock standard solutions of the elements at 1000 mg L^{-1}. Wavelengths used for Cu, Co, Ni, Zn, Cd and Pd determination were 213.598, 238.892, 231.604, 202.548, 214.439 and 340.458 nm, respectively, whereas for Ge the line at 209.426 nm was used. The operating conditions were optimized to obtain the maximum signal intensity, and between each sample, a rinse solution constituted by 2 % v/v of HNO_3 was used in order to avoid memory effects.

2.7. Preparation of the MWCNT-LPd catalyst

Since the extraction tests demonstrated that MWCNT-L is able to extract Pd(II) from the tested metal ion mixture in a quantitative manner, the atomically precise heterogeneous MWCNT-LPd catalyst, to be used in the ORR experiments, was prepared using the same mother solution employed in the extraction tests (Pd(II), Cu(II), Co(II), Ni(II), Zn (II) and Cd(II), each in 1.0 mM, pH 4), the same ligand:metal ion 1:1 M ratio and keeping the suspension under stirring for 10 days. Then the solid was recovered by filtration, washed with water and dried under reduced pressure at room temperature in the presence of a desiccant (NaOH) until constant weight. Quantitative extraction of Pd(II) was ascertained by ICP-OES analysis of the residual solution after filtration of MWCNT-LPd. Accordingly, the catalyst contains Pd(II) in 0.182 mmol/g. The BET surface area of MWCNT-LPd (61.4 m^2/g) was determined by N_2 adsorption.

2.8. Determination of specific surface area of MWCNT-LPd

The specific surface area of the catalyst (61.4 m^2/g) was determined by N_2 adsorption at 77 K using a 3Flex Micromeritics gas adsorption analyser and applying the Brunauer−Emmett−Teller (BET) equation to the adsorption data. Before recording the isotherm, the sample was held at 353 K for 2 h under nitrogen flow into the FlowPrep Micromeritics apparatus and then at 353 K for 2 h under vacuum directly into the measuring instrument.

2.9. SEM, STEM and XPS surface analysis

The MWCNT-LPd catalyst was investigated by Scanning Electron Microscopy equipped with Energy Dispersive X-ray detector (SEM-EDS). SEM images were obtained with a Hitachi SU3800 SEM equipped with an UltimMax Oxford instrument EDS detector and AZtecLive. Samples were drop casted from a water dispersion on an aluminium holder and dried under an N_2 flow. EDS analysis was performed using an acceleration voltage of 5 kV and a working distance of 10 mm. Scanning Transmission Electron Microscopy (STEM) analysis was performed using a double aberration corrected JEOL NeoArm 200F cold field emission with a 200 kV acceleration voltage. High Angle Annular Dark Field (HAADF) images were acquired using a annular detector within a collection semiangle range from 68 mrad to 280 mrad. STEM EDS acquisition was done using a dual JEOL detector with collection angle 1.8 str. Data were acquired and analysed using Gatan Digital Micrograph GMS3.6 SI Quantification suite. Samples for STEM investigations were deposited on TEM Cu grids supported by lacey carbon film following a previously described procedures [87]. X-ray photoelectron spectroscopy (XPS) spectra were performed using a glassy carbon substrate and an Al Kα radiation with an energy of 44 eV (XPS survey) and 22 eV (high resolution XPS spectra). A TA10 X-ray source and a HA100 hemispherical analyser (VSW Scientific Instrument Limited, Manchester, UK) with a 12-channel detector were used. As a reference for obtaining the heteroatom binding energies we used the C 1s transition at 284.8 eV [88] and data were analysed using the CasaXPS software. The background was subtracted using Shirley's method [89] and the peaks were fitted using mixed Gaussian–Lorentzian (GL30) components.

2.10. Electrochemical and ORR study

Cyclic voltammetry (CV), linear sweep voltammetry (LSV) and chronoamperometry experiments were conducted with an AUTOLAB PGSTAT12 interfaced with NOVA software from Metrohm Autolab using a three-electrode cell consisting of (i) a reference Ag/AgCl/sat. KCl electrode with a potential of +197 mV with respect to the normal hydrogen electrode (NHE) (ii) a platinum wire as counter electrode and (iii) a ring-disk working electrode from Pine Instrument Co. consisting of a glassy carbon (GC) disk insert (∅ = 5.5 mm; A = 0.238 cm^2) and a Pt ring (∅inner = 6.50 mm, ∅outer = 8.50 mm, A = 0.236 cm^2) with a theoretical collection efficiency (N) of 38.3 %. A tailored electrochemical cell in which the working electrode (consisting of a 1.5 cm diameter GC disc) is placed on the bottom was used to perform electrochemical tests using Nafion-free inks. The RRDE working electrodes were mechanically polished with 0.05 μm alumina and sonicated for 5 min in milliQ water. The Pt ring electrode was electropolished in a 0.5 M H_2SO_4 solution scanning the potential at 100 mV s^{-1} between −0.20 and + 1.15 V until a reproducible curve was obtained. Experiments with the rotating ring-disk electrode were performed using a modulated speed rotator (MSR) 636A from Pine Instrument. The glass cell was filled with a 0.1 M KOH and the solution was purged with nitrogen for 15 min to remove oxygen and obtain the blank solutions. The electrolyte solution was saturated with oxygen for 20 min.

CVs for the ORR study were obtained by scanning the potential between +0.1 and −0.80 V at a potential scan rate of 10 mV s^{-1}. LSV were obtained in the potential range from +0.1 to −0.80 V at a rotation speed

of 1600 rpm and a scan rate of 10 mV s^{-1} (for the modified GC electrode) while the Pt ring electrode was held at +0.50 V. As provided by the RRDE technique, the ring current was recorded simultaneously with the disk current. RRDE calibration experiment was conducted recording LSV at 1600 rpm of an oxygen-free $K_3Fe(CN)_6$ solution (10 mM) in 0.1 M KCl at a scan rate of 10 mV s^{-1} in the potential range from +0.60 V to −0.60 V (GC disk) and applying a constant potential of +0.6 V at the Pt ring. The ratio between the current recorded at the disc and at the ring gives the experimental collection efficiency ($N = I_{ring}/I_{disk}$) [90]. The electron transfer number exchanged per O_2 molecule (n) was calculated using the equation $n = 4I_{disk}/(I_{disk} + I_{ring}/N)$ [91].

Moreover, the Koutecky-Levich equation was used to estimate H_2O selectivity by recording LSV at different rotation rates. The average number of exchanged electrons (n) was calculated from the slope of the J^{-1} *vs.* $\omega^{-1/2}$ plot according to the following equation:

$$\frac{1}{J} = \frac{1}{JK} + \frac{1}{0.62nFCD^{2/3}\nu^{-1/6}\omega^{1/2}} \text{ with } K_f = 0.62FCD^{2/3}\nu^{-1/6}$$

where J_K is the kinetic current density (mA/cm^2), n is the number of exchanged electrons per O_2 molecule, F is the Faraday's constant (96487 C mol^{-1}), C is the oxygen concentration in the electrolyte (1.15 x 10^{-3} mol/dm^3), D is the oxygen diffusion coefficient (1.95 x 10^{-5} cm^2/s), ν is the electrolyte kinematic viscosity (0.008977 cm^2/s) and ω is the angular frequency of rotation (rad s^{-1}). The electrochemical surface area (ECSA) was evaluated by the electrochemical double-layer capacitance (Cdl) method [92]. The latter was estimated by performing cyclic voltammetry (CV) in a non-faradic current region [93]. The CV were carried out at multiple scan rates (800, 400, 200, 100, 50, 25, 10, 5) mV s^{-1}.

Electrochemical impedance spectroscopy (EIS) experiments were conducted using a FRA32 module and a conventional three-electrode system. After determining the open-circuit potential (OCP), the impedance spectra were acquired by sweeping the frequency from 10 kHz to 1 mHz at 10 points per decade, with an AC amplitude of 5 mV around the OCP. All data were recorded in single-sine mode. The measurements were conducted by rotating at 1600 rpm. The impedance spectra were fitted with Nova 2.1 by building the equivalent circuit. Finally durability tests were done for MWCNT-L Pd recording 15,000 LSV curves at the scan rate of 50 mVs^{-1} (Fig. S17). The reported LSV was acquired at the scan rate of 10 mV s^{-1}.

Modification of the GC disk working electrode with the catalysts was performed by preparing an ink consisting of (% m/m): catalyst 2 %, water 52 %, EtOH 26 % and Nafion® 20 %. The resulting ink containing about 2 mg of catalysts was sonicated for 30 min and drop-casted onto the glassy carbon disk electrode (10 μL). The modified GC electrode was then dried at room temperature. A sample of the dried material deposited on the electrode was mineralized using a microwave-assisted digestion (CEM MARS Xpress) using a 1:1 (v:v) mixture of suprapure HNO_3, obtained by sub-boiling distillation, and suprapure HCl. The resulting mixture was then diluted with MilliQ water, spiked with 0.5 ppm Ge, used as an internal standard, and analysed. Accordingly, the mass of Pd per unit electrode surface was found to be 0.015 μg/cm^2.

All potentials shown in the results were converted to reversible hydrogen electrode (RHE), unless otherwise specified.

3. Results and discussion

The objective of this work is to obtain an efficient atomically precise heterogeneous Pd(II)-based catalyst for the ORR reaction in alkaline media using as the source of Pd(II) an acidic solution containing several metal ions in addition to Pd(II), as occurs in wastewater containing palladium, and as the extractant (the second component of the catalyst), the functionalized MWCNT-L, according to a spontaneous process occurring in very environmentally friendly conditions (room temperature, water, unprotected atmosphere). For this to be feasible, the ligand (HL) used to functionalize the MWCNTs must be able to form stable complexes with Pd(II) in both acidic (for Pd(II) extraction) and alkaline (for ORR at high pH) solutions.

The catalyst itself must be stable under these conditions. Before assessing the robustness of the catalysts, however, it is advisable to assess the stability of the Pd(II) complex in this wide pH range. Even when the ligand forms complexes of high stability, demetallation processes may occur, especially under the stress that the catalysts are subjected during use. When this occurs, it commonly consists in a modest alteration of the catalyst due to the reduction of Pd(II) to Pd(0) leading to the formation of Pd nanoparticles. These, in turn, can be endowed with good catalytic activity towards the same reaction so that the catalyst continues to function efficiently [58,67,70]. A preliminary screening of the Pd(II) complex was performed by means of UV–Vis spectroscopy to assess its stability in the pH range 1.1–12.0 (see section 3.2.).

A second crucial point to achieve the objective of this works is the selectivity of the MWCNT-L material in extracting Pd(II) from a mixture of metal ions. This is strictly correlated to the coordination selectivity of the coordinative unit of the ligand attached to the nanotubes in MWCNT-L, as it has been shown that basicity and coordination properties of the coordinative unit are fundamentally retained upon attachment onto graphene surfaces via π-π stacking interaction of the pyrimidine anchor group (6-amino-3,4-dihydro-3-methyl-5-nitroso-4-oxopyrimidine) while the latter experience a substantial shutdown of its own properties [58,59,94]. A crystallographic characterization of the complexes $[Cu(HL)Cl_2]$, $[Zn(HL)Cl_2]$ and $[Pd(HL)Cl]Cl{\cdot}5H_2O$ (see section 3.1.) excluded the participation of the pyrimidine group of HL in metal coordination and showed that these complexes are conformationally well-suitable for adhesion of the pyrimidine group on the surface of MWCNTs. The solution study, performed on the Cu(II) and Pd(II) complexes, confirmed that in $[Cu(HL)]^{2+}$ and $[Pd(HL)]^{2+}$ the pyrimidine group of HL does not participate in metal binding (see section 3.2.). Nevertheless, the deprotonated form of HL (L^-) does it in $[CuL]^+$ and $[PdL]^+$ starting from pH 6 and above, but this is irrelevant for the functioning of the MWCNT-L material as extractant of metal ions and for the preparation of the MWCNT-LPd catalyst because both will be carried out in an acidic solution and, as just mentioned, the pyrimidine functionalities become unreactive once they are stacked onto the MWCNT surface.

The mixture of metal ions we considered for this study includes Pd (II), Cu(II), Co(II), Ni(II), Zn(II) and Cd(II), which are the most recurring cations present in Pd-containing wastewater [95–101], in the presence of dissolved chlorides and at the working pH 4. Other metal ions, such as alkaline and alkaline earth, are commonly present but do not have significant affinity for polyamine ligands, so they are not expected to interfere with Pd(II) coordination and were not included in our model solution. Taking into account the well-known trends of thermodynamic stability of transition metal complexes with polyamine ligands [82], we could safely assume that the stability of the Pd(II) complex with HL is largely greater than that of complexes of the other metal ions, but we were not able to verify this assumption since we were not able to determine the stability constant of the Pd(II) complex because it is too high and the complexation reaction is affected by the typical slowness of this metal ion. Nevertheless, the ability of MWCNT-L to selectively extract Pd(II) from the above-mentioned mixture of metal ions was assessed by means of a practical extraction test (see section 3.3.)

3.1. Crystallographic study

$[Cu(HL)Cl_2]$ and $[Zn(HL)Cl_2]$ complexes are isomorphous and crystallize in the orthorhombic system, space group $P2_12_12_1$. Selected bond angles and distances are listed in Table S2 while drawings of the asymmetric unit content are shown in Fig. 2a and b. In the two structures, the Cu(II) and Zn(II) complexes show almost equal conformations, with the metal centre 5-coordinated by the tertiary nitrogen and the two

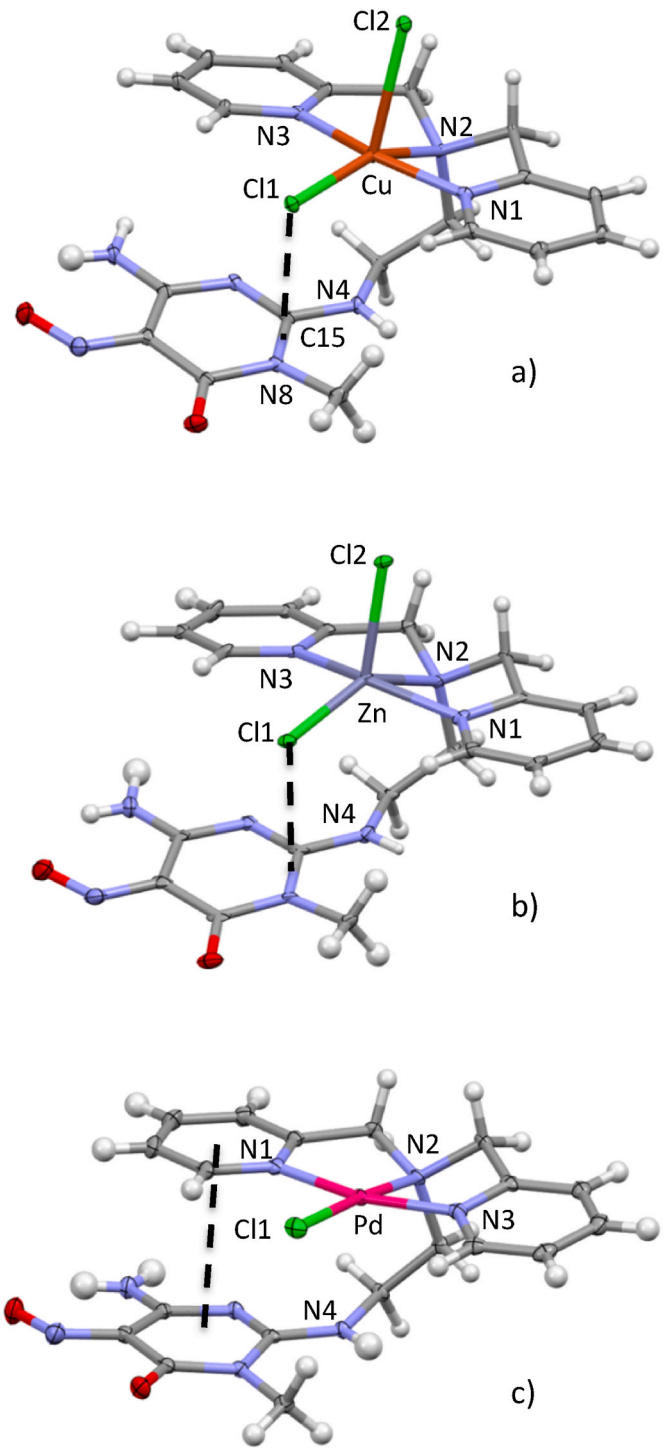

Fig. 2. a) Drawings of the metal complexes in the crystal structures of a) [Cu(HL)Cl_2], b) [Zn(HL)Cl_2] and c) [Pd(HL)Cl]Cl·5H_2O.

pyridine nitrogen atoms of the ligand and by two exogenous chloride ions. The coordination environment of Cu(II) is better described as a distorted square pyramid, with the basal plane defined by the three nitrogen atoms and Cl1 (deviations in the range 0.0152(6) Å and 0.241(2) Å). The copper atom is located 0.2975(4) Å above this plane and displaced toward the apical position occupied by Cl2. The Cu-Cl2 bond forms an angle of 8.72(3) deg with the normal to the basal plane. The pyrimidine pendant folds up in such a way that the Cl1 is placed almost above the C15-N8 bond of the heteroaromatic group at short distance from it (3.26 Å, distance Cl1•••C15-N8 bond centroid). As a consequence of this folding, the N4 nitrogen atom can be considered to occupy a sixth long-distance coordination position (Cu•••N4, 3.139(2) Å).

In [Zn(HL)Cl_2], the overall conformation assumed by the ligand is rather similar to that shown in [Cu(HL)Cl_2], but the coordination sphere of Zn(II) is intermediate between a square pyramid and a trigonal bipyramid with the two pyridine nitrogen atoms defining the axial bonds. Interestingly, the Cl1 ion maintains the same position relative to the pyrimidine group as found in the Cu(II) complex, actually being 3.25 Å from the centroid of the C15-N8 bond. On the other hand, due to the change in coordination environment, the N4 nitrogen atom is at longer distance from the metal centre than in the copper complex (Zn•••N4, 3.318(5) Å).

In [Pd(HL)Cl]Cl·5H_2O, the Pd(II) metal centre is found in the expected square planar coordination geometry, where the 4-coordination is determined by the tertiary nitrogen and the two pyridine nitrogen atoms of the ligand and by a chloride ion. The overall neutrality is guaranteed by the presence of an external chloride anion and the crystalline packing is assisted by the contribution of the H bonds formed by the five cocrystallized water molecules. Selected bond angles and distances for metal coordination are listed in Table S2, while a drawing of the $[Pd(HL)Cl]^+$ complex is shown in Fig. 2c. Also here the ligand is folded, but this time the pyrimidine group gives rise to a π-stacking interaction with one of the pyridine groups (N1) (3.18 Å interplanar distance and 3.67 Å distance between the centroids of pyridine and pyrimidine groups). By this way, the N4 atom is now at 3.087(2) Å from the metal centre.

3.2. Ligand protonation and formation of metal complexes

As mentioned above, it was not possible to determine the stability constants of the complexes formed by HL with Pd(II), owing to thermodynamic and kinetic complications, but we were able to determine the stability constants of the complexes formed with Cu(II) which coupled with the data of selective extraction of Pd(II) in the presence of Cu(II) (and other metal ions) furnish a rough estimation of the stability of Pd(II) complexes. Furthermore, the resolved speciation of the Cu(II)/HL system can be used as a reference for the analysis of the Pd(II)/HL one.

The ligand protonation constants and the stability constants of Cu(II) complexes were determined by means of potentiometric (pH-metric) titrations and are listed in Table 1. HL bears a weak acidic group, the NH group (red in Fig. 1a) of the bridge connecting the pyrimidine residues to the binding unit, which deprotonates in fairly alkaline solution to form the negatively charged L^- species (log$K$ = 11.88 in Table 1 corresponds to protonation of this species). On lowering the solution pH, the neutral HL, which is almost the unique species in the pH range 7.5–10.5, undergoes three successive protonation steps (Table 1, Fig. S3c).

UV–Vis spectra recorded in the pH range 0.8–12.6 (Figs. S3a and b) show that important spectral modifications are observed below pH 3 and above pH 11 (Fig. S3c) when protonation/deprotonation equilibria

Table 1
Equilibrium constants for ligand protonation and formation of Cu(II) complexes in 0.1 M NMe_4Cl at 298.1 K. Values in parentheses are standard deviation in the last significant figure.

Equilibrium	log$K$
$L^- + H^+ = HL$	11.88(1)
$HL + H^+ = H_2L^+$	5.82(3)
$H_2L^+ + H^+ = H_3L^{2+}$	3.04(3)
$H_3L^{2+} + H^+ = H_4L^{3+}$	2.17(3)
$L^- + Cu^{2+} = [CuL]^+$	16.9(1)
$HL + Cu^{2+} = [Cu(HL)]^{2+}$	12.29(6)
$H_2L^+ + Cu^{2+} = [Cu(H_2L)]^{3+}$	8.77(7)
$[LCu]^+ + OH^- = [CuLOH]$	3.3(1)

involve the very sensitive pyrimidine chromophore. In the higher pH range (pH > 11) the spectral change is due to the above mentioned equilibrium ($L^- + H^+ = HL$, log$K = 11.88$) involving NH group (red in Fig. 1a) directly connected to the pyrimidine residues, while in the lower pH range (pH < 3) protonation ($H_3L^{2+} + H^+ = H_4L^{3+}$, log$K = 2.17$) involves the nitroso pyrimidine group (the oxygen atom of the NO group) [50,102]. In the intermediate pH region, where protonation occurs on the not-sensitive or less-sensitive nitrogen atoms of the binding unit (Fig. 1) the spectral variation is modest (Fig. S3).

The stability constants of the complexes formed by HL with Cu(II) are listed in Table 1. As can be seen, both HL and its deprotonated (L^-) and protonated (H_2L^+) species bind Cu(II). The $[Cu(HL)]^{2+}$ complex has a stability (log$K = 12.29$ for $HL + Cu^{2+} = [Cu(HL)]^{2+}$) that compares well with the stability of Cu(II) complexes of triamine ligands similar to the coordinative unit of HL [82]. Deprotonation of $[Cu(HL)]^{2+}$ gives rise to a significant enhancement of complex stability (log$K = 16.9$ for $L^- + Cu^{2+} = [CuL]^+$) that can be ascribed to the involvement in metal coordination of the deprotonated, negatively charged nitrogen atom. The UV–Vis spectral variation with pH of this complex system (Fig. 3) helps to interpret the complexation processes. In the acidic region, the ligand (Figs. S3a and c) and its Cu(II) complex (Fig. 3a–c) show similar behaviours: the 257 nm absorbance decreases while.

The 330 nm absorbance increases with increasing pH: the nitroso group of the pyrimidine moiety which is protonated in both free ligand and the complex releases the proton going toward less acidic solutions. Starting from pH 6 onwards, the complex reverses these trends (Fig. 3b and c), similarly to what HL does above pH 11 (Figs. S3b and c) when the NH group (red in Fig. 1a) connecting the pyrimidine residues to the coordination unit deprotonates (this is clearly shown by the trend of the 330 nm absorbances depicted in Fig. 3d), that is, deprotonation of this NH group in the complex occurs at much lower pH due to coordination of the resulting negatively-charge nitrogen atom to Cu(II).

The UV–Vis spectral behaviour of Pd(II) complexes (Fig. 4) shows strong similarities to that reported for Cu(II) complexes (Fig. 3) which are characterized by protonation of the nitroso group of the pyrimidine residue below pH 3 and deprotonation above pH 6 of the NH group (red in Fig. 1a) connecting the pyrimidine with the linker that joins it to the coordinative unit. Also in this case, a similar displacement toward low pH of the deprotonation of this NH group in the complex

Compared to the free ligand, which deprotonates above pH 11, can reasonably be attributed to coordination to Pd(II) of the resulting negatively charged N atom. Even if, as already commented, these phenomena do not occur when the pyrimidine residue is stacked on graphene surfaces and then they are irrelevant for the MWCNT-LPd catalyst, it is intriguing to understand how the $[Pd(HL)Cl]^+$ complex rearranges its structure when it forms its deprotonated species. Unfortunately, all our attempts to crystallize this deprotonated complex to try to characterize it by XRD were unsuccessful. So, in the absence of direct crystallographic information and by analogy to the general characteristics of Pd(II) complexes with other similar tripodal ligands, which are square planar and involve only three donors atoms [103–105], we can suppose that, upon deprotonation of $[Pd(HL)Cl]^+$, the square planar structure of the complex is preserved while one of the coordinated pyridine groups is replaced by the deprotonated nitrogen atom.

3.3. Absorption of metal ions by MWCNT-L

As already said, the ability of polyamine ligands to form complexes of higher thermodynamic stability with Pd(II) than with any other metal ion of the model mixture we studied (Cu(II), Co(II), Ni(II), Zn(II), Cd(II)) is a recurrent observation [82]. This is promising for achieving selective extraction of Pd(II) from this mixture of ions. Nevertheless, it is advisable not to place too much trust in similar considerations based merely on the thermodynamic stability of the individual complexes because under real extraction conditions various effects can intervene that can frustrate these expectations, e.g. effects due to different complexation kinetics of the different metal ions or to permanent or transitory formation of heteropolynuclear complexes.

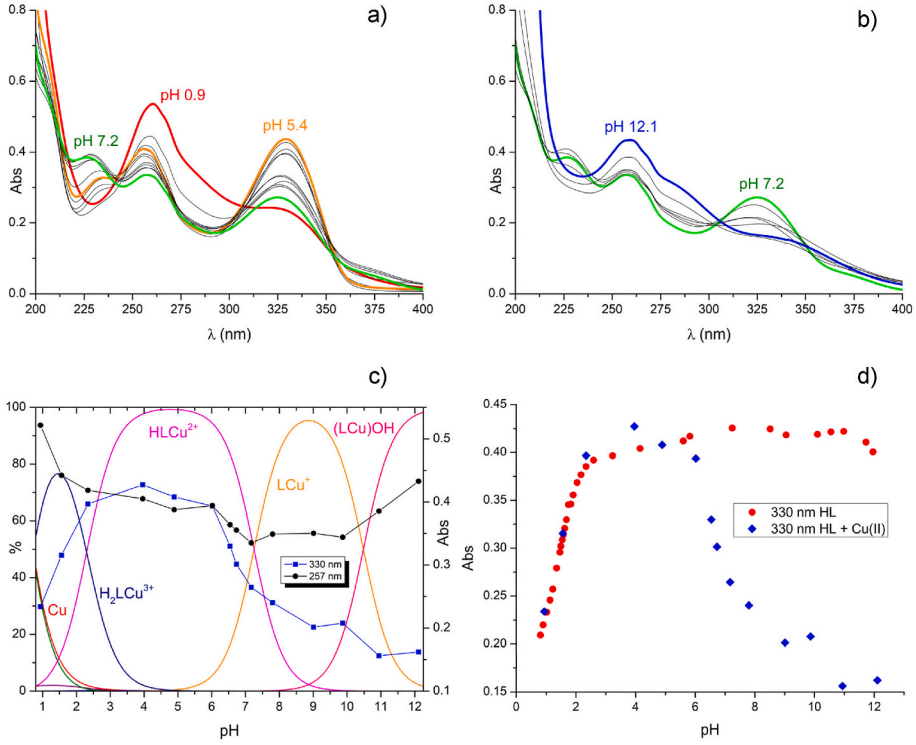

Fig. 3. UV–Vis absorption spectra of the Cu(II)/HL complex system in the pH ranges 0.9–7.2 (a) and 7.2–12.1 (b). (c) Variation with pH of the 257 nm and 330 nm absorbances superimposed to the distribution diagram of the complexes formed. (d) Comparison between the absorbances at 330 nm of HL and of its Cu(II) complexes. $[HL] = [Cu^{2+}] = 2 \bullet 10^{-5}$ M.

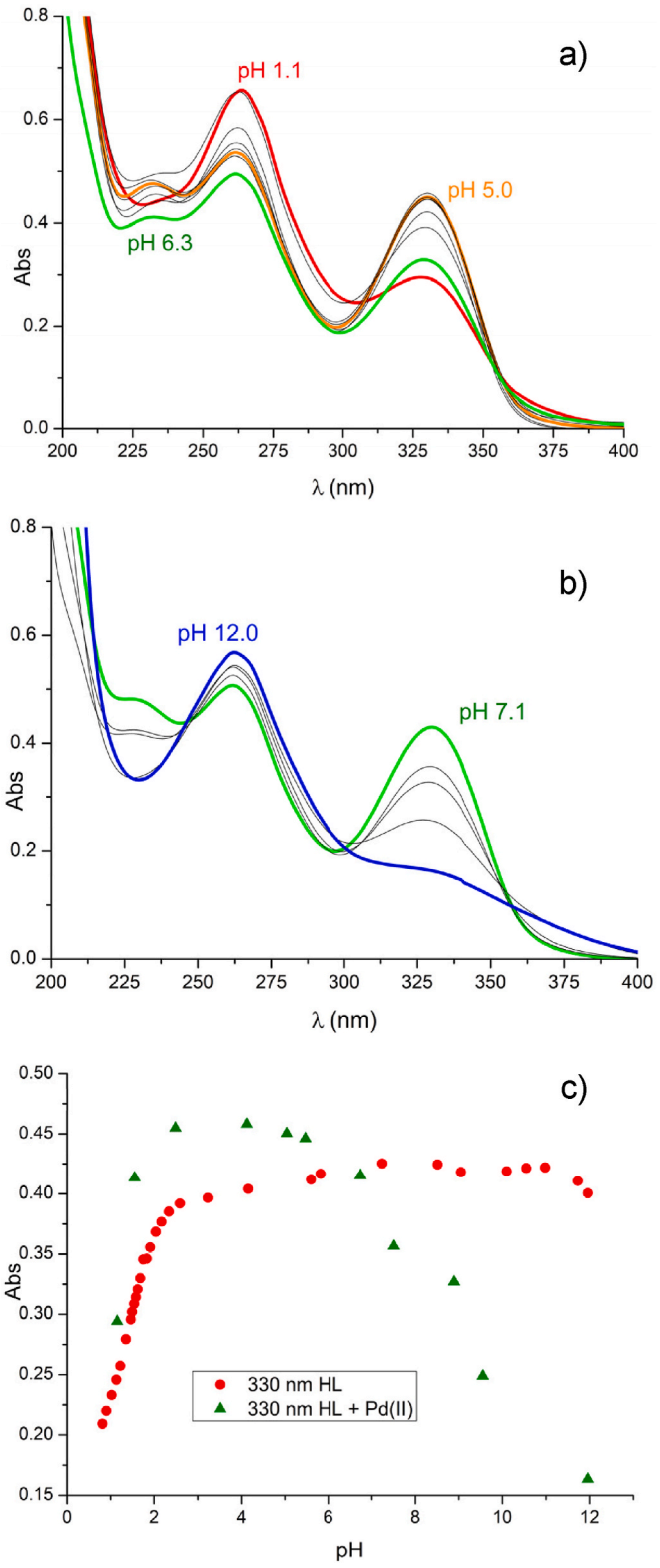

Fig. 4. UV–Vis absorption spectra of the Pd(II)/HL complex system in the pH ranges 1.1–6.3 (a) and 7.1–12.0 (b). (c) Comparison between the absorbances at 330 nm of HL and of its Pd(II) complexes. [HL] = $[Pd^{2+}] = 2 \bullet 10^{-5}$ M.

Pragmatically, we performed direct extraction experiments by using a solution at pH 4 containing Pd(II), Cu(II), Co(II), Ni(II), Zn(II) and Cd (II), 1 mM each, in the presence of 14 mM chloride (counterions of metals), by using 1 equivalent of L (L in MWCNT-L) with respect to one metal ion and checking how the extraction proceeded over time. The results reported in Fig. 5 show that selective and complete extraction of Pd(II) is achieved in 10 days at 298 K, which means that in this stint of time the MWCNT-LPd catalyst forms spontaneously on site and is ready for use in the ORR.

Data in Fig. 5 refer to the amount of metal ions remained in solution after filtration of the adsorbent. After 2 h from the start of the extraction experiment, 5 % of Pd(II), 66 % of Cu(II) and about 100 % of all other metal ions remained in solution, that is the MWCNT-L material had removed more than 1 eq. of metal ions compared to the ligand available on its surface. In the following days, the quantity of Cu(II) present in solution progressively increases, until it returns to 100 % at the end of the experiment, while free Pd(II) decreases until it almost disappears. All other metal ions remained at approximately 100 % throughout the experiment (Fig. 5): their inability to compete with Pd(II) and Cu(II) is in accordance with the lower stability of the complexes they form with amino-ligands [82].

The observed behaviour can be rationalized by considering the thermodynamic and kinetic properties of the complexes involved. Pd(II) is known to form much more stable complexes with amino-ligands than the other metal ions in our study, but its complexation reactions are typically slow. The only metal ion capable of offering some initial competition to Pd(II) is Cu(II), thanks to the good stability of its complex and the speed of its complexation reaction, but over time (a few days) the sluggish Pd(II) prevails, cancels the effects of its kinetic slowness and affirms its thermodynamic superiority.

This information allows us to make some interesting considerations on the metal ion sequestration capability of HL and the thermodynamic stability of the Pd(II) complex. Based on the stability constants determined for Cu(II) complexes (Table 1) and with the use of the Hyss program [106], we can calculate than 1 eq of HL is sufficient to sequester 98 % of Cu(II) at a total concentration of metal of 10 μM at pH 2.5, the sequestration capability increasing at higher pH's (Fig. S4). Therefore, even more interestingly for our purposes, the sequestration capacity of HL towards Pd(II) must be much higher since Pd(II) is selectively and exhaustively sequestered in the presence of Cu(II). Moreover, considering that, according to the extraction results, in a solution containing HL, Pd(II), Cu(II) and the other metal ions, all in the same 1.0 mM concentration, 100 % of the ligand is coordinated to Pd(II), the stability constant of the Pd(II) complex must be at least 3 orders of magnitude higher than the stability constant of the Cu(II) complex formed in the experimental conditions of the extraction experiment.

An intriguing point is the extraction of more than 1 eq. of metal ions

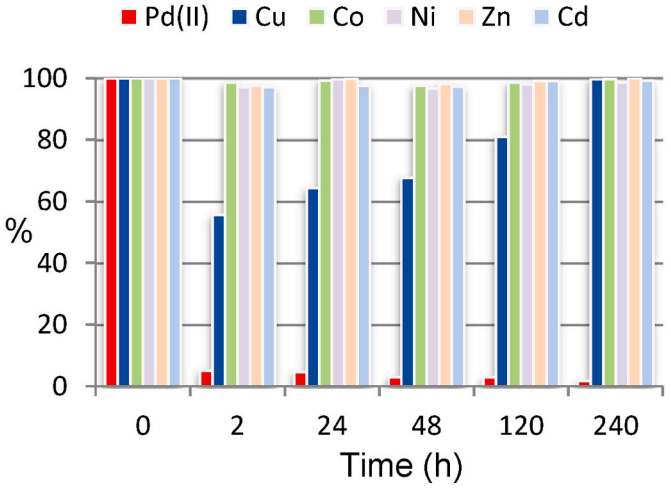

Fig. 5. Adsorption of metal ions by MWCNT-L over time. Percentages are referred to the amount of metal ions remained in solution after adsorption. Initial $[M^{2+}] = 1.0$ mM, 1 eq. of HL, pH 4, 298 K. Time 0 h correspond to the solution composition before the addition of MWCNT-L.

(Pd(II) and Cu(II)) at the beginning of this experiment. Several factors could contribute to this occurrence. A first possibility is the adsorption of Pd(II) in the form of $PdCl_4^{2-}$ which is the main species of Pd(II) under our experimental conditions ($[Cl^-]$ = 14 mM). In fact, it is known that $PdCl_4^{2-}$ is adsorbed on graphene surfaces via C−dπ interactions with the arene centres of these sorbents [107,108]. Thus, part of $PdCl_4^{2-}$ is expected to be initially adsorbed on the surface of MWCNT-L not covered by HL and some could be adsorbed even by the covered part. We have no information on the latter, but we cannot exclude that even the surface paved with pyrimidine groups is capable of doing so. A second possibility is the transient formation of heteropolynuclear complexes: Pd(II) and Cu(II) are simultaneously coordinated by a single ligand molecule of MWCNT-L, although it seems unlikely that three donor atoms could share two (or more) metals ions. Another possibility is that some $PdCl_4^{2-}$ can be drawn out of the solution as the counterion of the complexes initially formed by MWCNT-L, despite the concentration of free chloride is approximately 10 times that of $PdCl_4^{2-}$.

We do not know if all, and to what extent, these possibilities contribute to the observed phenomenon, nor whether there are others, but it is clear that in the end only Pd(II) is present in the MWCNT-LPd catalyst. The only metal ion capable of offering some initial competition is Cu(II), thanks to the good stability of its complex and the speed of the complexation reaction.

3.4. SEM, STEM and XPS analysis

The SEM images of MWCNT, MWCNT-L and MWCNT-LPd (Fig. S5) do not show any substantial morphological difference between pristine and functionalized MWCNTs, in agreement with the mild supramolecular approach employed in the preparation of the catalyst, while the BET surface area determined by N_2 adsorption (Fig. S6) has decreased from 117 m^2/g for MWCNT to 61.4 m^2/g for MWCNT-LPd, as commonly observed [109,67–69] when carbon materials with graphene surfaces are functionalized with pyrimidine derivatives analogous to HL. As expected, significant differences are observed in the EDS spectra (Fig. S7). Indeed, the spectra of pristine MWCNTs show only the C signal and a minimal presence of oxygen, while for MWCNT-L a small Kα signal at 0.39 keV denotes the presence of N introduced by the amino-ligand and for the MWCNT-LPd a Lα1 Pd signal at 2.62 keV is observed which confirms the presence of Pd. Chlorine, which is expected to accompany Pd(II) as Cl^- [50,67], is also detected in the EDS analysis of the catalyst.

No trace of other metals can be found in the EDS spectra of MWCNT-LPd in agreement with the observed ability of MWCNT-L to selectively extract Pd(II) from the tested mixture of metal ions (Pd(II), Cu(II), Co (II), Ni(II), Zn(II) and Cd(II)). The EDS map of MWCNT-LPd (Fig. 6) demonstrates a uniform distribution of Pd across the sample, confirming that the supramolecular approach used in the preparation of this atomically precise catalyst effectively achieves a homogeneous dispersion of the catalytic centres.

HAADF STEM images, whose intensity is proportional to $Z^{1.7}$, with Z being the atomic number of the elements imaged, reveal the presence of Pd over lighter elements. Although the visibility of individual atoms on the surface of MWCNTs was reduced by the electrostatic charging of the sample during the experiment, the acquired images show the presence of

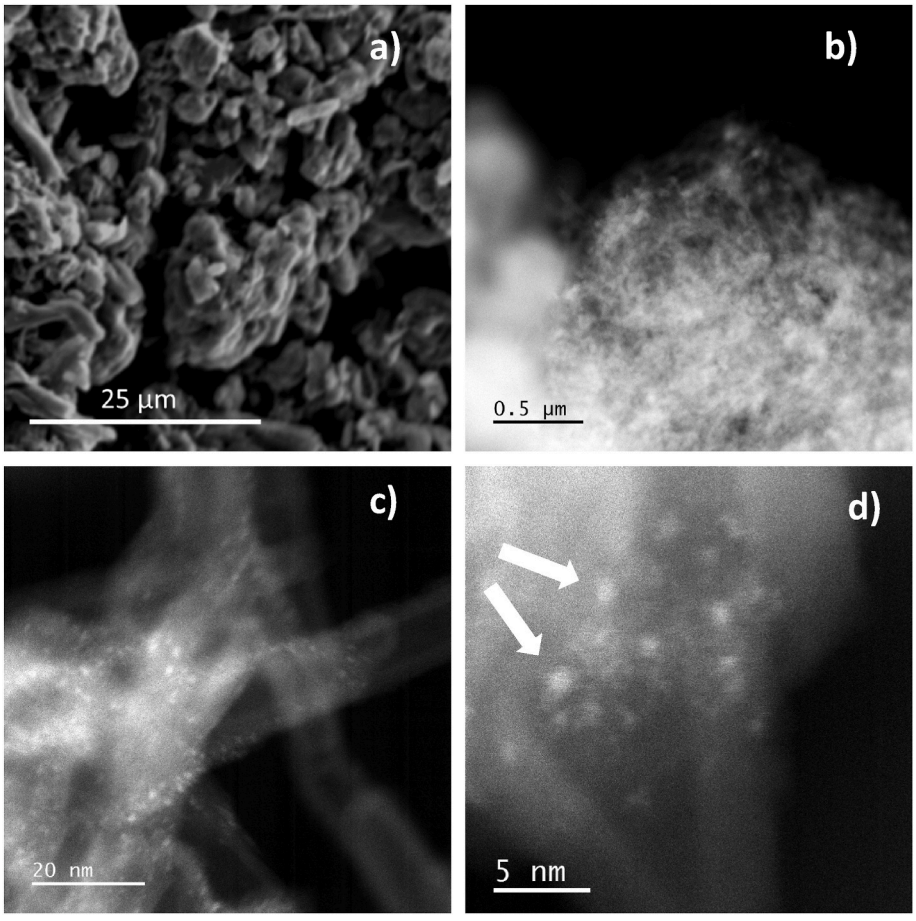

Fig. 6. Multiscale images of the MWCNT-LPd catalyst showing: a) grains overview by SEM secondary electron imaging; b) edges of a single grain revealing a dense network of MWCNTs; c) individual MWCNTs at higher magnification decorated with bright patches of Pd(II) complex agglomerates highlighted by Z-contrast; d) high resolution details of Pd(II) patches with brighter areas with overlapping Pd complexes (two of them are indicated by the white arrows) and individual layers of Pd(II) complexes between and around the patches. Images b), c) and d) where obtained by HAADF STEM imaging.

single layers of palladium atoms surrounding small white patches with dimensions ranging from a few nanometers to subnanometer size and representing Pd clusters on the MWCNTs (Fig. 6c and d). These small patches are mainly visible along the lateral edges of the nanotubes and at the intersections between nanotubes (Fig. 6c) and could be generated, at least in part, by the overlapping of Pd atoms or very small aggregates that are close to each other but kept separated by the ligand. The lack of crystallinity and the weak contrast indicate that Pd is not forming nanoparticles but rather 2D clusters on the surface. The presence of ligand molecules (as revealed by the overlap of N and Cl with Pd in STEM EDS maps and spectrum (Fig. S8) indicates that Pd is bound to them, as confirmed by the XPS analysis below, that is all palladium is present as Pd(II) complex.

It is not surprising that we found small aggregates of palladium complexes in the MWCNT-LPd since some multilayer formation was expected to occur under the experimental conditions adopted to coat the MWCNTs with ligand molecules (see 2.5. Preparation of the MWCNT-L material).

XPS analysis was performed on the MWCNT-LPd catalyst before and after electrochemical testing. The XPS survey is shown in Fig. S9 where the signals corresponding to C, O, Pd, N, Cl can be identified. In agreement with the EDS spectral data, no metals other than Pd were found in the samples. Fig. 7ashows the high-resolution XPS spectra obtained in the Pd region (3d transition of palladium, binding energy from 360 eV to 325 eV). Peak fitting reveals a single component corresponding to Pd(II) coordinated to N donors (binding energies: $3d_{5/2}$, 338.8 eV; $3d_{3/2}$, 344.1 eV) [110–112]. No presence of reduced metal Pd (0) was found, neither in the original material nor in the catalyst analysed after electrochemical tests. This confirms the robustness of the method used for functionalising MWCNTs and the stability of the catalyst obtained (see below).

More insight into the nature of the catalysts is provided by the analysis of the XPS spectra of Cl (Fig. 7b). MWCNT-LPd shows a signal in the Cl range consisting of two peaks, assigned to the electrons of the $2p_{3/2}$ and $2p_{1/2}$ states of Cl, each of which is composed of two peaks that can be attributed to the presence of two different chloride anions: one coordinated to Pd(II) and the second acting as a counterion [67]. Same situation was found in the crystal structure of the Pd(II) complex of this ligand (Fig. 2c), thus highlighting that the coordination environment of Pd(II) in the free complex is preserved when the latter is anchored to MWCNTs.

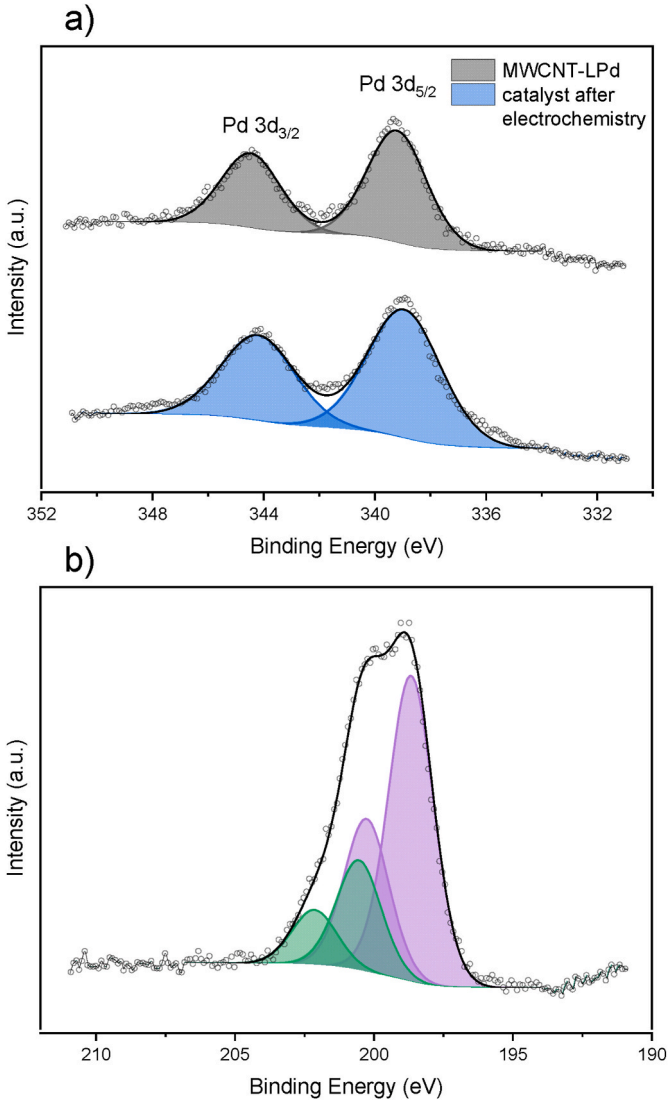

Fig. 7. High resolution XPS spectra of MWCNT-LPd in: a) the Pd 3d region, b) the Cl 2p region. Black lines: global fits of experimental data; black dots: experimental data.

3.5. Oxygen reduction reaction

The catalytic performance of MWCNT-LPd for oxygen reduction reaction (ORR) was evaluated under a range of electrochemical conditions, providing key insights into the reaction kinetics and mechanisms. The evaluation was carried out by determining the onset potential (E_{on}), the half-wave potential ($E_{1/2}$), and the number of exchanged electrons (n). In particular, the onset potential reflects the initial energy barrier for the ORR, and the half-wave potential is a commonly used benchmark to assess the overall efficiency of the catalyst in driving the ORR [113]. The third parameter, the number of exchanged electrons (n), is essential in distinguishing the ORR pathways. In alkaline media, the reaction can proceed via two primary mechanisms: the 4-electron pathway, in which O_2 is reduced directly to OH^-, or the 2-electron pathway, leading to the production of hydrogen peroxide (HO_2^-) [114]. In other contexts, hydrogen peroxide is explored as an environmentally friendly oxidant, but inside fuel cells its generation is highly undesirable.

Therefore, a higher n-value, corresponding to the 4-electron pathway, is preferred to maximize energy output and long-term stability of the fuel cell [115].

Cyclic voltammetry (CV) in 0.1 M KOH solution purged with either N_2 or O_2 performed on modified GC electrodes are shown in Fig. S10. In the O_2 saturated solutions, it is easy to recognise the irreversible peak of oxygen reduction while a redox couple at the potential of 0.65 V (vs RHE) is present both in O_2 and N_2 purged solutions. As also seen in a previous work, this redox couple is characteristic of the pyrimidine anchor group used for functionalization of the MWCNT [50]. Fig. 8a shows the linear sweep voltammetry curves in the KOH 0.1 M oxygen saturated solution obtained with the rotating-ring disk electrode. The LSV curve of MWCNT-LPd is shifted to less negative potentials, with better onset potential and higher current density respect to MWCNT-L.

This evidence shows the important catalytic activity of palladium-based atomically precise electrocatalysts. Moreover, the functionalized MWCNTs show better catalytic activity, with curves shifted towards more positive potentials and higher limiting current densities than non-functionalized MWCNTs and bare glassy carbon electrodes [50]. Table S3 resumes all the electrochemical results concerning the onset potential, the half-wave potential and the number of exchanged electrons per oxygen molecule.

Furthermore, the currents recorded at the ring of the RRDE electrode were examined, offering a deeper understanding of the factors influencing catalyst performance. Both the ring and disk current densities are illustrated in Fig. S11. Linear sweep voltammetry (LSV) ring-disk currents in a $K_3Fe(CN)_6$ solution performed to determine the experimental collection efficiency (N) are shown in Fig. S12. The experimental values

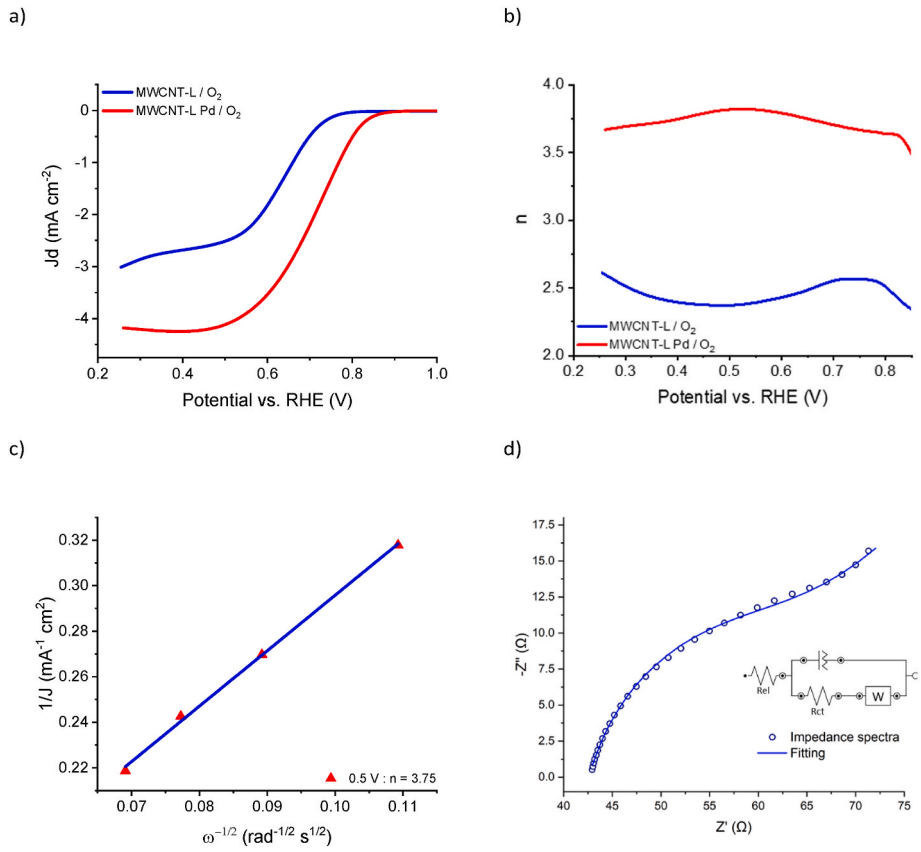

Fig. 8. ORR electrocatalytic performance, KOH 0.1 M, O_2 saturated solution, 1600 rpm rotation rate, 10 mV s^{-1} scan rate. a) ORR polarization curves (disk current densities). b) RRDE number of exchanged electrons per O_2 molecule (n) as function of the potential applied at the RRDE working electrode. c) K–L plot of the MWCNT-LPd catalyst. d) Nyquist plot of MWCNT-LPd. Impedance spectra acquired by sweeping the frequency from 10 kHz to 1 mHz at 10 points per decade, with an AC amplitude of 5 mV around the OCP while rotating at 1600 rpm. Fitting obtained with a Randles equivalent circuit ($\chi^2 = 5.71\ 10^{-4}$).

of N are in agreement with the theoretical value of 38.3 %. Fig. 8b shows the number of exchanged electrons per O_2 molecule determined by RRDE experiments. For the palladium-free hybrid MWCNT-L material (studied for comparison), the number of exchanged electrons is close to 2, indicating a predominant formation of hydrogen peroxide. This is a common behaviour for carbon-based materials [116]. In contrast, for the MWCNT-LPd catalyst, the electron transfer number approaches 4, accounting for a significant shift toward the more desirable 4-electron pathway, where oxygen is almost exclusively converted into water. The validity of the RRDE results was further examined by the Koutecky-Levich method for the MWCNT-L Pd catalyst. The J^{-1} *vs.* $\omega^{-1/2}$ plot is shown in Fig. 8c while ORR curves obtained at different rotation rates are shown in Fig. S13. The numbers of exchanged electrons were calculated from the slopes of the K-L plot yielding 3.75. In addition, we evaluated the electrochemical surface area (ECSA) using the electrochemical double-layer capacitance (Cdl) method. CVs were held in a 0.1 V potential window from the open-circuit potential (OCP) [93]. Thus, a potential range of (−0.1 - 0.1) V vs. Ag/AgCl KCl sat. was chosen after finding a OCP value approximately equal to 0 V (Fig. S14a). In this region, the current is attributed to charge and discharge phenomena of the electric double layer at the electrode-electrolyte interface, which behaves like a capacitor [117].

By plotting the current (I_c) against the scan rate (v_s) we obtain a straight line whose slope is Cdl (Fig. S14b). The ECSA of the MWCNT-LPd is determined by dividing Cdl by the specific capacitance of the glassy carbon electrode (0.3 mF/cm^2 in KOH 0.1 M) [118]. The ECSA value obtained is 0.353 cm^2. To better understand the result, the ECSA value was expressed in a different unit of measurement, dividing it by the mass of the loaded metal and expressing the final result in m^2/g. The value of ECSA obtained equal to 99.04 m^2/g is comparable to commercial Pt/C reported in the literature [119].

Furthermore, an EIS analysis was conducted at an amplitude of 5 mV over a frequency range from 100 kHz to 1 mHz. Fig. 8d shows Nyquist plots for MWCNT-LPd catalyst while Fig. S15 shows the Bode plot. The impedance spectra was fitted by building the equivalent circuit of the system (Fig. 8d), where the electrical elements are arranged in the so-called Randles circuit. The first resistance represents the resistance of the electrolyte (Rel), while the second one is the resistance for the charge transfer (Rct). The other elements are a constant phase element (CPEdl) for the double layer, and a Warburg (Wd) for the semi-infinite diffusion of the ionic species through the diffusion layer. The value of Rel (42.6 Ω) is consistent with the value obtained by IR drop. The catalyst charge transfer impedance, Rct, is 24.8 Ω, which is close to Pt/C catalysts with a similar metal loading [120].

A preliminary short-term (10 min) stability test was conducted using the RRDE in galvanostatic mode to simulate a half-cell environment. The MWCNT-LPd catalyst demonstrated high activity and stability, which are crucial for improving ORR efficiency. The modified GC disk electrode was maintained at a potential of 0.36 V (vs RHE), while the ring electrode was held at +1.46 V for a duration of 600 s at a rotation speed of 1600 rpm. The galvanostatic results, presented in Fig. S16, demonstrate that the ring-disk current density values remained stable throughout the experiment, indicating the durability and robustness of the catalyst under continuous operation. Durability test was done on MWCNT-LPd according to an accelerated degradation test. A 15,000 LSV repetitions were conducted in 0.1 M KOH solution with a scan rate of 50 mV s^{-1}. Cycles number 1, 2,000, 5,000, 10,000, and 15,000 are shown in Fig. S17 A reduction of only 6 % in limiting current was detected after 15,000 cycles. Furthermore, no significant change in the onset potential was observed, which indicates the high stability of the catalyst. In

addition, the catalyst recovered after the electrochemical tests was subjected to SEM and XPS analysis. No morphological difference is visible in SEM images of MWCNT-LPd before (Fig. S5) and after electrochemical testing (Fig. S18). The EDS spectrum in Fig. S7d highlight the robustness of the catalyst, with no detectable loss of palladium during the electrochemical test. Additionally, signals corresponding to fluorine and sulphur are observed, originating from the sulfonated tetrafluoroethylene-based fluoropolymer-copolymer Nafion added during ink preparation. Furthermore, the XPS spectra shown in Fig. 7a confirm that Pd remains stable as Pd(II), no significant difference is observed in the spectra recorded before and after the electrochemical tests (compare the grey line with the blue line). This indicates that the catalyst retains its structural integrity and homogeneity under operational conditions.

4. Conclusions

We have successfully achieved the goal of this study, that is, we have prepared an efficient Pd(II)-based catalyst for ORR in alkaline media using, as the Pd(II) source, a mixture of metal ions representative of Pd-containing wastewater. This atomically precise catalyst, MWCNT-LPd, while containing a low precious metal content (1.94 % in the catalyst, 0.015 μg/cm^2 mass of Pd per unit electrode surface) offers a performance comparable to that of traditional (and very expensive) bulk platinum electrodes. MWCNT-LPd loaded electrodes give rise to ORRs with 90 % H_2O production (4 e^- process), onset potential (E_{on}) of 0.846 V (vs RHE) and half-wave potential ($E_{1/2}$) of 0.657 V which are within the high performance range exhibited by analogous atomically precise electrocatalysts [50,72] as well as by non-PGM and PGM carbon-based electrocatalysts, including commercial products, showing 4 e^- ORR patters and E_{on} and $E_{1/2}$ potentials in the ranges 0.38–1.1 V and 0.42–0.94 V, respectively [121–124]. This performance is maintained for at least 80 min and no significant morphological and chemical changes were observed after electrochemical tests, indicating a great robustness of the catalyst.

These results strengthen the belief that atomically precise catalysts may represent a valid and economical alternative to bulk platinum electrodes for ORR in fuel cells. Moreover, we have shown that the catalyst can be generated *in situ* by quantitatively and selectively extracting Pd(II) from wastewater.

Treatment of waste and their transformation into a high value-added material, as in our case a catalyst to be implemented in fuel cells for the production of green energy, is an example of circular economy that considers environmental protection an essential condition for sustainable development. In line with the above, we also demonstrated that both the hybrid material (MWCNT-L) used to prepare the catalyst (MWCNT-LPd) and the catalyst itself can be prepared under very environmentally friendly conditions (room temperature, water as solvent, air as atmosphere) using a supramolecular functionalization of MWCNTs which, despite involving only non-covalent interactions, leads to a very robust catalyst.

All in all, we have illustrated here a simple and successful strategy to contribute to the development of cost-effective solutions for clean energy production, based on green processes and waste recovery and paying special attention to environmental protection.

CRediT authorship contribution statement

Marco Bonechi: Writing – original draft, Visualization, Investigation. **Carlotta Cappanni:** Visualization, Investigation. **Pietro Gentilesca:** Visualization, Investigation. **Carla Bazzicalupi:** Writing – original draft, Visualization, Investigation. **Walter Giurlani:** Visualization, Investigation. **Massimo Innocenti:** Supervision, Funding acquisition, Conceptualization. **Leonardo Lari:** Investigation. **Francesco Montanari:** Validation, Investigation. **Matteo Savastano:** Validation, Supervision, Conceptualization. **Mirko Severi:** Writing – original draft, Investigation, Conceptualization. **Antonio Bianchi:** Writing – review & editing, Supervision, Funding acquisition, Conceptualization.

Declaration of competing interest

The authors declare that they have no known competing financial interests or personal relationships that could have appeared to influence the work reported in this paper.

Acknowledgements

The following projects are gratefully acknowledged: 1) GRAFENEX, Prog. n. F/310131/01–05/X56 funded by the Italian Ministry of Enterprises and Made in Italy; 2) FUTURO, 2022NW4P2T CUP B53D23013890006 PRIN2022 funded by the Italian Ministry of University and Research and NextGenerationEU; 3) FREEGALVAN, CUPST 27716.29122023.042000059, LINEA 1 - PRFESR 2021–2027 OP1 OS1 Azione 1.1.4 Bando n.1; 4) P.U.L.S.E, CUPST 27717.29122023.043000271, LINEA 2 - PRFESR 2021–2027 OP1 OS1 Azione 1.1.4 Bando n.1. L.L would like to acknowledge EPSRC (UK) capital infrastructure grant EP/S033394/1.

Appendix B. Supplementary data

Supplementary data to this article can be found online at https://doi.org/10.1016/j.jpowsour.2025.236661.

Data availability

Data will be made available on request.

References

[1] S. van Ewijk, J. Stegemann, An Introduction to Waste Management and Circular Economy, UCL Press, London, 2023. https://discovery.ucl.ac.uk/id/eprint/10182591/1/An-Introduction-to-Waste-Management-and-Circular-Economy.pdf.
[2] M.A.P. Mahmud, S.H. Farjana, C. Lang, N. Huda, Green Energy: a Sustainable Future, Academic Press (Elsevier), London, 2023.
[3] T.-Z. Ang, M. Salem, M. Kamarol, H.S. Das, M.A. Nazari, N. Prabaharan, Energy Strategy Rev. 43 (2022) 100939.
[4] Y. Guanglei, Z. Dongla, C. Dongqin, Z. Guoxing, Innovation 5 (2024) 100582.
[5] https://chemistry-europe.onlinelibrary.wiley.com/doi/10.1002/chem.202401403..
[6] Y. Wang, Y. Liu, Z. Xu, K. Yin, Y. Zhou, J. Zhang, P. Cui, S. Ma, Y. Wang, Z. Zhu, Renew. Sustain. Energy Rev. 189 (2024) 114015.
[7] I. Staffell, D. Scamman, A. Velazquez Abad, P. Balcombe, P.E. Dodds, P. Ekins, N. Shah, K.R. Ward, Energy Environ. Sci. 12 (2019) 463–491.
[8] G. Hoogers, F. Kreith (Eds.), Fuel Cell Technology Handbook, CRC Press, Boca Raton, 2002.
[9] B.C.H. Steele, A. Heinzel, Nature 414 (2001) 345–352.
[10] M. Gazzotti, A. Stefani, M. Bonechi, W. Giurlani, M. Innocenti, C. Fontanesi, Molecules 25 (2020) 3988.
[11] R. Kawondera, M. Bonechi, I. Maccioni, W. Giurlani, T. Salzillo, E. Venuti, D. Mishra, C. Fontanesi, M. Innocenti, G. Mehlana, W. Mtangi, Front. Chem. 11 (2023) 1215619.
[12] A. Kabata-Pendias, A.B. Mukherjee, Trace Elements from Soil to Human, Springer, Berlin, 2007.
[13] C. Melber, D. Keller, I. Mangelsdorf, Palladium, World Health Organization, Geneva, 2002. https://iris.who.int/bitstream/handle/10665/42401/WHO_EHC_226.pdf?sequence=1&isAllowed=y.
[14] J.W. Moore, L. Hall, K. Campbell, J. Stara, J. Environ. Health Perspect. 10 (1975) 63–71.
[15] S.A. Cotton, Chemistry of precious metals. Blackie Academic and Professional, Chapman & Hall, London, 1997.
[16] A.O. Adeeyo, O.S. Bello, O.S. Agboola, R.O. Adeeyo, J.A. Oyetade, M.A. Alabi, J. N. Edokpayi, R. Makungo, Water Reuse 13 (2023) 134–161.
[17] A.T. Nakhjiri, H. Sanaeepur, A.E. Amooghin A, M.M.A. Shirazi, Desalination 527 (2022) 115510.
[18] D. Bozejewicz, M.A. Kaczorowska, K. Witt, Desalination Water Treat. 246 (2022) 12–24.
[19] S. McCarthy, A. Lee Wei Jie, D.C. Braddock, A. Serpe, J.D.E.T. Wilton-Ely, Molecules 26 (2021) 5217.
[20] T. Wongsawa, N. Traiwongsa, U. Pancharoen, K. Nootong, Hydrometallurgy 198 (2020) 105488.

[21] S.K. Padamata, A.S. Yasinskiy, P.V. Polyakov, E.A. Pavlov, D. Yu Varyukhin, Metall. Mater. Trans. B 51 (2020) 2413–2435.
[22] K. Avarmaa, L. Klemettinen, H. O'Brien, P. Taskinen, Miner. Eng. 133 (2019) 95–102.
[23] M.N. Le, M.S. Lee, Miner. Process. Extr. Metall. Rev. 42 (2020) 335–354.
[24] M. Sethurajan, E.D. van Hullebusch, D. Fontana, A. Akcil, H. Deveci, B. Batinic, J. P. Leal, T.A. Gasche, M. Ali Kucuker, K. Kuchta, I.F.F. Neto, H.M.V.M. Soares, A. Chmielarz, Crit. Rev. Environ. Sci. Technol. 49 (2019) 212–275.
[25] H. Li, J. Eksteen, E. Oraby, Resour. Conserv. Recycl. 139 (2018) 122–139.
[26] K.K. Singh, R. Ruhela, A. Das, M. Kumar, A.K. Singh, R.C. Hubli, P.N. Bajaj, J. Environ. Chem. Eng. 3 (2015) 95–103.
[27] G. Pfrepper, R. Pfrepper, M. Knothe, Hydrometallurgy 21 (1989) 293–304.
[28] B. Gupta, I. Singh, Hydrometallurgy 134–135 (2013) 11–18.
[29] A.P. Paiva, O. Ortet, G.I. Carvalho, C.A. Nogueira, Hydrometallurgy 171 (2017) 394–401.
[30] O. Lanaridi, M. Schnürch, A. Limbeck, K. Schröder, ChemSusChem 15 (2022) e202102262.
[31] J. Bauwens, L.S. Rocha, H.M. Soares, Environ. Sci. Pollut. Res. 29 (2022) 76907–76918.
[32] R.M. Izatt, S.R. Izatt, N.E. Izatt, K.E. Krakowiak, R.L. Bruening, L. Navarro, Green Chem. 17 (2015) 2236–2245.
[33] Q. Xiao, L.J. Song, X.Y. Wang, H.W. Xu, L.L. He, Q.J. Li, S.D. Ding, Sep. Purif. Technol. 280 (2022) 119805.
[34] C. Ianăşi, E.M. Picioruş, R. Nicola, A.M. Putz, A. Negrea, M. Ciopec, A. Len, L. Almásy, Soft Mater. 20 (2022) S68–S75.
[35] X. He, S. Minelli, A. Vertova, A. Minguzzi, Curr. Opin. Electrochem. 36 (2022) 101166.
[36] J. Hou, M. Yang, C. Ke, G. Wei, C. Priest, Z. Qiao, G. Wu, J. Zhang, Energy (Calg.) 2 (2020) 100023.
[37] J.K. Nørskov, J. Rossmeisl, A. Logadottir, L. Lindqvist, J.R. Kitchin, T. Bligaard, H. Jónsson, J. Phys. Chem. B 108 (2004) 17886–17892.
[38] F. Nosheen, T. Anwar, A. Siddique, N. Hussain, Front. Chem. 7 (2019) 456.
[39] H.A. Miller, M. Bellini, W. Oberhauser, X. Deng, H. Chen, Q. He, M. Passaponti, M. Innocenti, R. Yang, F. Sun, Z. Jiang, F. Vizza, Phys. Chem. Chem. Phys. 18 (2016) 33142–33151.
[40] M. Kiani, X.Q. Tian, W. Zhang, Coord. Chem. Rev. 441 (2021) 213954.
[41] X. Huang, Y. Wang, W. Li, Y. Hou, Sci. China Chem. 60 (2017) 1494–1507.
[42] H.A. Miller, M. Bevilacqua, J. Filippi, A. Lavacchi, A. Marchionni, M. Marelli, S. Moneti, W. Oberhauser, E. Vesselli, M. InnocentiM, F. Vizza, J. Mater. Chem. A 1 (2013) 13337–13347.
[43] P. Jiao, D. Ye, C. Zhu, S. Wu, C. Qin, C. An, N. Hu, Q. Deng, Nanoscale 14 (2022) 14322–14340.
[44] M.D. Bhatt, J.Y. Lee, Energy Fuels 34 (2020) 6634–6695.
[45] L. Xue, L. Guolei, Z. Han, S. Kuizhao, W. Linna, C. Jing, A. Saira, C. Yue Cao, S. Weimeng, W. Fagang, B. Awais, Energies 16 (2023) 128.
[46] D. Iglesias, A. Giuliani, M. Melchionna, S. Marchesan, A. Criado, L. Nasi, M. Bevilacqua, C. Tavagnacco, F. Vizza, M. Prato, P. Fornasiero, Chem 4 (2018) 106–123.
[47] G. Tuci, C. Zafferoni, A. Rossin, A. Milella, L. Luconi, M. Innocenti, L. Truong Phuoc, C. Duong-Viet, C. Pham-Huu, G. Giambastiani, Chem. Mater. 26 (2014) 3460–3470.
[48] Z. Yan, L. Gao, C. Dai, M. Zhang, X. Lv, P.K. Shen, Int. J. Hydrogen Energy 43 (2018) 3705–3715.
[49] H. Li, H. Zhao, G. Yan, G. Huang, C. Ge, M. Forsyth, P.C. Howlett, X. Wang X, J. Fang, Small 20 (2024) 2304844.
[50] V. Monini, M. Bonechi, C. Bazzicalupi, A. Bianchi, P. Gentilesca, V. Giurlani, M. Innocenti, A. Meoli, G.M. Romano, M. Savastano, Dalton Trans. 53 (2024) 2487–2500.
[51] L. Yan, P. Li, Q. Zhu, A. Kumar, K. Sun, S. Tian, X. Sun, Chem 9 (2023) 280–342.
[52] A. Kumar, S. Ibraheem, T.A. Nguyen, R.K. Gupta, T. Maiyalagan, G. Yasin, Coord. Chem. Rev. 446 (2021) 214122.
[53] A. Kumar, Y. Zhang, W. Liu, X. Sun, Coord. Chem. Rev. 402 (2020) 213047.
[54] A. Kumar, V.K. Vashistha, D.K. Das, Coord. Chem. Rev. 431 (2021) 213678.
[55] M. Wang, H. Zhang, Y. Liu, Y. Pan, J. Energy Chem. 72 (2022) 56–72.
[56] S. Ji, Y. Chen, X. Wang, Z. Zhang, D. Wang, Y. Li, Chem. Rev. 120 (2020) 11900–11955.
[57] B. Singh, V. Sharma, R.P. Gaikwad, M.B. Gawande, P. Fornasiero, R. Zboril, R. Zboril, Small 17 (2021) e2006473.
[58] J. García-Martín, R. López-Garzón, M.L. Godino-Salido, M.D. Gutiérrez-Valero, P. Arranz-Mascarós, R. Cuesta, F. Carrasco-Marín, Langmuir 21 (2005) 6908–6914.
[59] M.L. Godino-Salido, A. Santiago-Medina, R. Lopez-Garzon, M.D. Gutierrez-Valero, P. Arranz-Mascaros, M.D. Lopez de la Torre, M. Domingo-Garcia, F. J. Lopez-Garzon, Appl. Surf. Sci. 387 (2016) 128–138.
[60] M.D. Gutierrez-Valero, M.L. Godino-Salido, P. Arranz-Mascaros, R. Lopez-Garzon, R. Cuesta, J. Garcia-Martin, Langmuir 23 (2007) 5995–6003.
[61] J. Garcia-Martin, R. Lopez-Garzon, M.L. Godino-Salido, R. Cuesta-Martos, M. D. Gutierrez-Valero, P. Arranz-Mascaros, H. Stoeckli-Evans, H. Eur. J. Inorg. Chem. 2005 (2005) 3093–3103.
[62] M. Savastano, P. Arranz-Mascaros, C. Bazzicalupi, M.P. Clares, M.L. Godino-Salido, L. Guijarro, M.D. Gutierrez-Valero, A. Bianchi, E. Garcia-Espan, R. Lopez-Garzon, ACS Omega 2 (2017) 3868–3877.
[63] M. Savastano, P. Arranz-Mascaros, C. Bazzicalupi, A. Bianchi, C. Giorgi, M. L. Godino-Salido, M.D. Gutierrez-Valero, R. Lopez-Garzon, RSC Adv. 4 (2014) 58505–58513.
[64] P. Arranz, A. Bianchi, R. Cuesta, C. Giorgi, M.L. Godino, M.D. Gutierrez, R. Lopez, A. Santiago, Inorg. Chem. 49 (2010) 9321–9332.
[65] M. Savastano, P. Arranz-Mascarós, M.P. Clares, R. Cuesta, M.L. Godino-Salido, L. Guijarro, M.D. Gutiérrez-Valero, M. Inclán, A. Bianchi, E. García-España, R. López-Garzón, Molecules 24 (2019) 2714.
[66] M. Savastano, P. Arranz-Mascarós, C. Bazzicalupi, M.P. Clares, M.L. Godino-Salido, M.D. Gutiérrez-Valero, M. Inclán, A. Bianchi, E. García-España, R. López-Garzón, J. Catal. 353 (2017) 239–249.
[67] A.M. Valbuena-Rus, M. Savastano, P. Arranz-Mascarós, C. Bazzicalupi, M. P. Clares, M.L. Godino-Salido, M.D. Gutiérrez-Valero, M. Inclán, A. Bianchi, E. García-España, R. López-Garzón, Inorg. Chem. 61 (2022) 12610–12624.
[68] M.L. Godino-Salido, M.D. Gutiérrez-Valero, R. López-Garzón, P. Arranz-Mascarós, A. Santiago-Medina, M. Melguizo, M. Domingo-García, F.J. López-Garzón, V. K. Abdelkader-Fernández, C. Salinas-Martínez De Lecea, M.C. Román-Martínez, RSC Adv. 6 (2016) 58247–58259.
[69] A.M. Valbuena-Rus, M.D. Gutierrez-Valero, P. Arranz-Mascaros, R. Lopez-Garzon, M. Melguizo, J. Vernet-Garcia, M. Perez-Mendoza, M.L. Godino-Salido, Appl. Surf. Sci. 554 (2021) 149646.
[70] M. Savastano, M. Passaponti, W. Giurlani, L. Lari, A. Bianchi, M. Innocenti, Energies 13 (2020) 5539.
[71] M. Bonechi, W. Giurlani, M. Vizza, M. Savastano, A. Stefani, A. Bianchi, C. Fontanesi, M. Innocenti, Catalysts 11 (2021) 764.
[72] M. Passaponti, M. Savastano, M.P. Clares, M. Inclan, M. Lavacchi, A. Bianchi, E. Garcia-Espana, M. Innocenti, Inorg. Chem. 57 (2018) 14484–14488.
[73] M. Savastano, M. Passaponti, W. Giurlani, L. Lari, N. Calisi, E. Delgado-Pinar, E. Salvador-Serrano, E. Garcia-Espana, M. Innocenti, V.K. Lazarov, A. Bianchi, Inorg. Chim. Acta. 518 (2021) 120250.
[74] M. Savastano, C. Zoppi, A. Bianchi, C. Bazzicalupi, Inorg. Chim. Acta. 511 (2020) 119793.
[75] M. Savastano, C. Cappanni, C. Bazzicalupi, C. Lofrumento, A. Bianchi, Crystals 13 (2023) 823.
[76] C. Bazzicalupi, A. Bianchi, T. Biver, C. Giorgi, S. Santarelli, M. Savastano, Inorg. Chem. 53 (2014) 12215–12224.
[77] M. Savastano, M. Fiaschi, G. Ferraro, P. Gratteri, P. Mariani, A. Bianchi, C. Bazzicalupi, Molecules 25 (2020) 1355.
[78] M. Fontanelli, M. Micheloni, Proceedings of the 1st Spanish-Italian congress on thermodynamics of metal complexes, Diputación de Castellón: Castellón, Spain (1990) 41–43.
[79] G. Gran, Analyst (London) 77 (1952) 661–671.
[80] P. Gans, A. Sabatini, A. Vacca, Talanta 43 (1996) 1739–1753.
[81] C. Bazzicalupi, A. Bencini, A. Bianchi, A. Danesi, C. Giorgi, B. Valtancoli, Inorg. Chem. 48 (2009) 2391–2398.
[82] D.R. Burgess, NIST SRD 46. Critically Selected Stability Constants of Metal Complexes: Version 8.0 for Windows, National Institute of Standards and Technology, 2004, https://doi.org/10.18434/M32154.
[83] SADABS, Bruker AXS Inc., Madison (WI), USA, 2001.
[84] G.M. Sheldrick, Acta Crystallogr. A 64 (2008) 112–122.
[85] G.M. Sheldrick, Acta Crystallogr. C71 (2015) 3–8.
[86] C.F. Macrae, I. Sovago, S.J. Cottrell, P.T.A. Galek, P. McCabe, E. Pidcock, M. Platings, G.P. Shields, J.S. Stevens, M. Towler, P.A. Wood, J. Appl. Crystallogr. 53 (2020) 226–235.
[87] L. Lari, C.J. Nuttall, M.P. Copley, R.J. Potter, J. Simon, N. Mingo, D. Ozkaya, J. Phys. Conf. Ser. 522 (2014) 012040.
[88] G. Maccaferri, C. Zanardi, Z.Y. Xia, A. Kovtun, A. Liscio, F. Terzi, V. Palermo, R. Seeber, Carbon 120 (2017) 165–175.
[89] D.A. Shirley, Phys. Rev. B 5 (1972) 4709–4714.
[90] U.A. Paulus, T.J. Schmidt, H.A. Gasteiger, R.J. Behm, J. Electroanal. Chem. 495 (2001) 134–145.
[91] F. Si, Y. Zhang, L. Yan, J. Zhu, M. Xiao, C. Liu, W. Xing, J. Zhang, Electrochemical oxygen reduction reaction, in: W. Xing, G. Yin, J. Zhang (Eds.), Rotating Electrode Methods and Oxygen Reduction Electrocatalysts, Elsevier, 2014, pp. 133–170.
[92] T. Zhang, F. Wang, C. Yang, X. Han, C. Liang, Z. Zhang, Y. Li, A. Han, J. Liu, B. Liu, Chem Catal. 2 (2022) 836–852.
[93] C.C.L. McCrory, S. Jung, I.M. Ferrer, S.M. Chatman, J.C. Peters, T.F. Jaramillo, J. Am. Chem. Soc. 137 (2015) 4347–4357.
[94] R. López-Garzón, M.L. Godino-Salido, M.D. Gutiérrez-Valero, P. Arranz-Mascarós, M. Melguizo, C. García, M. Domingo-García, F.J. López-Garzón, Inorg. Chim. Acta. 417 (2014) 208–221.
[95] A.D. Pournara, J.-H. Tang, L. Yang, J.-T. Liu, X.-Y. Huang, M.-L. Feng, M. G. Kanatzidis, Chem. Mater. 36 (2024) 3013–3021.
[96] N.H. Zulkernain, N. Basant, C.C. Ng, K.M. Salari, S. Mallick, J. Mater. Cycles Waste Manag. 25 (2023) 2726–2752.
[97] L. Zhang, B. Li, P. Shao, X. Zhou, D. Li, Z. Hu, H. Dong, L. Yang, H. Shi, X. Luo, Environ. Res. 238 (2023) 117253.
[98] C.-S. Lee, H. Rho, N. Sharma, B. Jung, P. Westerhoff, ACS EST Water 3 (2023) 2481–2490.
[99] J. Guo, Y. Wu, Z. Wang, J. Yu, J.-R. Li, J. Mater. Sci. 57 (2022) 10886–10911.
[100] X. Zhang, Z. Chen, Z. Wan, C. Liu, R. He, X. Xie, Z. Huang, Int. J. Mol. Sci. 23 (2022) 12158.
[101] J. Cui, L. Zhang, J. Hazard Mater. 158 (2008) 228–256.
[102] P. Arranz Mascaros, C. Bazzicalupi, A. Bianchi, C. Giorgi, M.L. Godino Salido, M. D. Gutíerrez Valero, R. López Garzón, M. Savastano, J. Am. Chem. Soc. 135 (2013) 102–105.
[103] H.O. Oloyede, J.A.O. Woods, H. Gorls, W. Plass, A.O. Eseola, Polyhedron 159 (2019) 182–191.

[104] G. Ferguson, M. Parvez, Acta Crystallogr. Sect. B Struct. Crystallogr. Cryst. Chem. 35 (1979) 2207–2210.
[105] G. Ferguson, P.J. Roberts, Acta Crystallogr. Sect. B Struct. Crystallogr. Cryst. Chem. 34 (1978) 3083–3086.
[106] L. Alderighi, P. Gans, A. Ienco, D. Peters, A. Sabatini, A. Vacca, Coord. Chem. Rev. 184 (1999) 311–318.
[107] N.V. Vorob'ev-Desyatovskii, S.A. Kubyshkin, R.I. Ibragimova, V.V. Kaichev, Y. A. Dubrovskii, V.N. Babakov, D.A. Pichugina, Russ. J. Gen. Chem. 82 (2012) 384–397.
[108] P.A. Simonov, A.V. Romanenko, I.P. Prosvirin, E.M. Moroz, A.I. Boronin, A. L. Chuvilin, V.A. Likholobov, Carbon 35 (1997) 73–82.
[109] J. Garcia-Martin, M.L. Godino-Salido, R. Lopez-Garzon, M.D. Gutierrez-Valero, P. Arranz-Mascaros, H. Stoeckli-Evans, Eur. J. Inorg. Chem. 2008 (2008) 1095–1106.
[110] NIST X-ray Photoelectron Spectroscopy Database, NIST Standard Reference Database Number 20, National Institute of Standards and Technology, Gaithersburg MD, 20899, 2000, https://doi.org/10.18434/T4T88K.
[111] I.A. Zakharova, Ja V. Salyn, L.V. Tatjanenko, Yu Sh Mashkovsky, G. Ponticelli, J. Inorg. Biochem. 15 (1981) 89–92.
[112] M. Yamashita, I. MuraseI, Bull. Chem. Soc. Jpn. 58 (1985) 2697–2698.
[113] A.J. Bard, L.R. Faulkner, H.S. White, Electrochemical Methods: Fundamentals and Applications, third ed., Wiley, Hoboken, NJ, 2022.
[114] X. Ge, A. Sumboja, D. Wuu, T. An, B. Li, F.W.T. Goh, T.S.A. Hor, Y. Zong, Z. Liu, ACS Catal. 5 (2015) 4643–4667.
[115] L. Gubler, S.M. Dockheer, W.H. Koppenol, J. Electrochem. Soc. 158 (2011) B755–B769.
[116] M. Siddika, N. Hosen, R.H. Althomali, J.Y. Al-Humaidi, M.M. Rahman, M. A. Hasnat, Catalysts 14 (2024) 164.
[117] S.B. Davey, A.P. Cameron, K.G. Latham, S.W. Donne, Electrochim. Acta 386 (2021) 138416.
[118] Y. Yia, G. Weinberg, M. Prenzel, M. Greiner, S. Heumann, S. Becker, R. Schlögl, Catal. Today 295 (2017) 32–40.
[119] Y. Garsany, J. Ge, J. St-Pierre, R. Rocheleau, K.E. Swider-Lyons, J. Electrochem. Soc. 161 (2014) F628.
[120] E. Sonmez, B. Avci, N. Mohamed, H. Bermek, Eur. Chem. Biotechnol. J. 1 (2024) 11–26.
[121] W.-W. Zhao, W.-J. Niu, R.-J. Li, B.-X. Yu, C.-Y. Cai, F.-M. Wang, L.-Y. Xua, Inorg. Chem. Front. 12 (2025) 479–514.
[122] X. Qu, Y. Yan, Z. Zhang, B. Tian, S. Yin, X. Cheng, R. Huang, Y. Jiang, S. Sun, Chem. Eur J. 30 (2024) e202304003.
[123] X. Meng, X. Zhang, J. Rageloa, Z. Liu, W. Wang, J. Power Sources 567 (2023) 232988.
[124] C. Lafforgu, F. Maillard, V. Martin, L. Dubau, M. Chatenet, ACS Catal. 9 (2019) 5613–5622.